Master's Thesis

Binaural Beamforming for Hearing Aids Using Differential Microphone Arrays

conducted at
Signal Processing and Speech Communication Laboratory
Graz University of Technology, Austria

by
Laura Leucke, BSc
0973049

Supervisor:
Dipl.-Ing. Dr.techn. Martin Hagmüller

Graz, March 2018

Statutory Declaration

I declare that I have authored this thesis independently, that I have not used other than the declared sources/resources, and that I have explicitly marked all material which has been quoted either literally or by content from the used sources. The uploaded document is identic with the present Master's Thesis.

date (signature)

Eidesstattliche Erklärung

Ich erkläre an Eides statt, dass ich die vorliegende Arbeit selbstständig verfasst, andere als die angegebenen Quellen/Hilfsmittel nicht benutzt und die den benutzten Quellen wörtlich und inhaltlich entnommenen Stellen als solche kenntlich gemacht habe. Das in TUGRAZonline hochgeladene Textdokument ist mit der vorliegenden Diplomarbeit identisch.

Graz, am (Unterschrift)

Acknowledgement

I owe my deepest gratitude to my supervisor, Dr. Martin Hagmüller, who guided me with his knowledge and advice throughout my whole master's thesis. He gave me the opportunity for this thesis to focus on a topic I have been interested in. I greatly appreciate his patience and reliable support which allowed for a pleasant work.

I would like to express my heartfelt gratitude to my family, especially to my parents who gave me the opportunity to attend this master program. Furthermore, they provided advice and assistance during my whole studies.

Abstract

Modern hearing aids are designed to improve speech enhancement algorithms in terms of signal-to-noise ratio but interaural cue distortion may occur. Previous studies have been shown that speech intelligibility is increased if the target and interfering sources are perceived from different directions. Therefore, it is essential to preserve binaural cues in order to maintain the source localization. This thesis focuses on beamforming algorithms which increase speech intelligibility as well a preserving binaural cues by using differential microphone arrays. Differential microphone arrays are suitable for compact devices as they use a compact sensor arrangement. Furthermore, they are able to steer at one target direction over a wide frequency range while interfering sources can be suppressed from different directions. To increase binaural cue preservation different postfilter techniques are proposed. The evaluation of the provided algorithms is done by means of objective measures and a listening test. It is shown that all proposed structures can enhance the signal-to-noise ratio as well as suppressing interfering sources. Nevertheless, the hybrid structure of frequency dependence reveals the best results for these parameters. Although the binaural cues are preserved for all tested postfilters, the postfilter operating on a single microphone signal achieved the best results. However, the suppression of interfering sources is not optimal for this filter which leads to a trade-off between noise reduction and cue preservation.

Kurzfassung

Hörgeräte haben zum Ziel, die Sprachverständlichkeit für Hörgeräteträger zu verbessern. Dies geschieht meist mit Hilfe der Verbesserung des Signal-Rauschabstandes. Dadurch kann es jedoch zur Verschlechterung der Lokalisationswahrnehmung kommen. In verschiedenen Studien wurde gezeigt, dass die Sprachverständlichkeit deutlich verbessert werden kann, wenn Signal und Störgeräusch aus unterschiedlichen Richtungen wahrnehmbar sind. Aus diesem Grund ist es wichtig, die binauralen Unterschiede zu erhalten, damit die Lokalisation der Schallereignisse bestehen bleibt. Diese Masterarbeit beschäftigt sich mit unterschiedlichen Beamforming-Algorithmen auf Basis von differentiellen Mikrofonarrays, die zum Ziel haben, sowohl die Sprachverständlichkeit zu verbessern als auch die Lokalisation zu erhalten. DMAs haben den Vorteil, dass sie für den Einsatz in schmalen Gehäusen geeignet sind. Außerdem besitzen sie die Fähigkeit, Schallquellen aus einer bestimmten Richtung verzerrungsfrei aufzunehmen und dabei Störquellen aus einer anderen spezifizierten Richtung zu unterdrücken. Um die Lokalisationsschärfe zu erhalten, werden unterschiedliche Methoden zur Berechnung eines nachgestellten Filters beschrieben. Die Auswertung der gefilterten Signale erfolgt sowohl durch objektive Maße als auch durch einen Hörversuch. Es zeigt sich, dass die vorgestellten Algorithmen sowohl den Signal-Rauschabstand verbessern als auch Störgeräusche sehr gut unterdrücken. Die Hybrid-Struktur in Abhängigkeit von der Frequenz zeigt jedoch für diese Parameter die besten Ergebnisse. Mit den Ergebnissen des Hörversuches zeigt sich, dass es immer einen Konflikt zwischen Rauschunterdrückung und Erhaltung der Lokalisationsschärfe gibt.

Contents

1 Introduction **13**

1.1 Introduction . . . 13
1.2 Motivation . . . 13
1.3 Objective . . . 14
1.4 Outline . . . 14

2 Fundamentals **15**

2.1 Coordinate System . . . 15
2.2 Signal Model . . . 15
2.3 Beampattern . . . 17

3 Differential Microphone Array **19**

3.1 Introduction . . . 19
3.2 First-Order Differential Microphone Array . . . 20
3.2.1 Compensation Filter $H_L(\omega)$ . . . 21
3.2.2 Frequency Response of First-Order DMA . . . 22
3.3 Second-Order Differential Microphone Array for Hearing Aids . . . 23
3.3.1 Frequency Response of Second-Order DMA . . . 24
3.4 Adaptive First-Order Differential Microphone Array . . . 25
3.4.1 Optimum β . . . 26
3.4.2 Normalized Least Mean Square (NLMS) . . . 26
3.5 Adaptive Second-Order Differential Array for Hearing Aids . . . 27
3.5.1 Optimum α . . . 29
3.6 Hybrid Structure . . . 30

4 Fixed Beamformer for Hearing Aid Geometry **33**

4.1 Introduction to Circular Differential Microphone Array . . . 33
4.2 First-Order Circular Differential Array . . . 35
4.2.1 Frequency Response of First-Order CDMA . . . 36
4.3 Second-Order Beamformer for Hearing Aid Geometry . . . 36
4.3.1 Frequency Response of Second-Order Beamformer . . . 39

5 Postfilter **41**

5.1 Introduction . . . 41
5.2 Postfilter Estimation using Cardioids PF_{Card} . . . 41
5.3 Postfilter Estimation using Signal-to-Noise Ratio PF_{SNR} . . . 43
5.4 Postfilter Estimation using Fixed Beamformer PF_{6Mic} . . . 44
5.5 Postfilter Estimation using Coherence PF_{Coh} . . . 44
5.6 Postfilter Processing on One Microphone . . . 45

6 Evaluation **47**

6.1 Audio Data . . . 47
6.2 HRIR Database . . . 48
6.3 Evaluation of Signal-to-Noise Ratio . . . 48
6.4 Evaluation with PEASS-Software . . . 51

6.5 Perceptual Evaluation 54

7 Conclusion and Outlook **57**

A Results of Listening Test **61**

B Abbreviations **65**

C Symbols **67**

List of Figures

1.1 (a) A scenario with one listener, one target source $s_0(t)$ and interfering sources $v(t)$, (b) schematic of the geometry of the microphones on the users head [3]. . . 14

2.1 Three-dimensional Cartesian coordinate system. 15
2.2 Schematic of a uniform linear array with processing filter $H_m(\omega)$ [6]. 16

3.1 First-order DMA: (a) common structure [7], (b) different beampatterns for $f = 1000Hz$. 21
3.2 Frequency response of a first-order DMA with sensor spacing $\delta \approx 0.008m$: (a) without compensation filter, (b) with compensation filter, (c) with ideal compensation filter. 23
3.3 Second-order DMA: (a) common structure, (b) different beampatterns for $f = 1000Hz$. 24
3.4 Frequency response of a second-order DMA with sensor spacing $\delta \approx 0.008m$: (a) without compensation filter, (b) with compensation filter 25
3.5 Schematic of a first-order adaptive differential microphone array [7]. 25
3.6 Beampatterns of first-order ADMA: (a) forward- and backward-facing cardioid, (b) different beampattern for $f = 1000Hz$. 27
3.7 Block diagram of second-order adaptive differential microphone array [10]. 27
3.8 Schematic implementation of an adaptive second-order differential array using fixed delay elements but different sensor spacings δ. 28
3.9 Block diagram of second-order adaptive beamformer [10]. 28
3.10 Beampatterns of second-order ADMA: (a) cardioids of second-order ADMA, (b) different beampatterns for $f = 1000Hz$ 29
3.11 Schematic implementation of hybrid structure using first- and second-order ADMA [11]. 30
3.12 Low- and high-pass filter for hybrid structure. 30
3.13 Principle of the input level dependent directivity [11]. 31

4.1 Schematic of a circular differential array [12]. 33
4.2 Different beampatterns of a first-order CDMA for $f = 1000Hz$. 35
4.3 Frequency response of a first-order CDMA with radius $r = 0.01m$ 36
4.4 Schematic of the six microphones arranged at the artificial head: (a) view of the right side, (b) view from the top. 36
4.5 Beampatterns of second-order beamformer for hearing aid geometry for $f = 1000Hz$: (a) elevation angle $\phi = 0°$ and no symmetry constraint (b) elevation angle $\phi \approx 19°$ and with symmetry constraint. 37
4.6 Beampatterns of second-order beamformer for hearing aid geometry for $f = 1000Hz$: (a) elevation angle $\phi = 0$, (b) elevation angle $\phi \approx 19°$. 38
4.7 Beampattern of second-order beamformer for hearing aid geometry for $f = 1000Hz$. 38
4.8 Frequency response of a second-order beamformer for hearing aid geometry. . . . 39

5.1 Schematic of postfilter structure using forward- and backward-facing cardioid of DMA. 42

5.2 Spectrogram of left side: (a) forward cardioid, (b) backward cardioid, (c) static speech mask 42
5.3 Schematic of postfilter structure using SNR estimation. 43
5.4 Schematic of postfilter structure using an additional beamformer. 44
5.5 Schematic of postfilter structure using a coherence function. 45
5.6 Schematic of postfilter structure used on a single microphone signal for each side. 45

6.1 Brüel & Kjær artificial head with hearing aid dummy (right side) [3]. 48
6.2 Absolute values of errors for background signals over all input signals for each tested angle: (a) errors of original signal, (b) errors of all postfilters. 55
6.3 Errors of background signals over all input signals and tested angles : (a) result of original input signal (b) result of different postfilters. 55

A.1 Errors of background signals over all input signals for each tested angle: (a) result of original signal, (b) result of PF_{Card}, (c) result of $PF_{CardOne}$, (d) result of PF_{SNR}. 61
A.2 Errors of background signals over all input signals for each tested postfilter compared to the original input signals: (a) result of angle 90°, (b) result of angle 45°, (c) result of angle 0°, (d) result of angle −45°, (e) result of angle −90°. 62
A.3 Errors of speech signals over all angles: (a) overall result of all input signals, (b) overall result of each postfilter for all input signals, (c) result of vacuum cleaner interferer for each postfilter, (d) result of music interferer for each postfilter, (e) result of street-sound interferer for each postfilter. 63
A.4 Errors of background signals over all angles: (a) overall result of all input signals, (b) overall result of each postfilter for all input signals, (c) result of vacuum cleaner interferer for each postfilter, (d) result of music interferer for each postfilter, (e) result of street-sound interferer for each postfilter. 64

List of Tables

6.1 Definition of input signals and source directions. 47
6.2 Calculation of input SNR. 48
6.3 Evaluation of different adaptive beamformer. 49
6.4 Evaluation of different postfilters. 50
6.5 Evaluation of postfilters applied to a single microphone signal for each side. . . . 50
6.6 Calculation of input SNR. 51
6.7 Evaluation of different adaptive beamformer with PEASS Software. 52
6.8 Evaluation of different postfilters with PEASS Software. 52
6.9 Evaluation of postfilters applied to a single microphone signal for each side. . . . 53
6.10 Direction of different presented stimuli. 54
6.11 Possible Angles of error observation. 54

1 Introduction

„Nicht Sehen trennt von den Dingen. Nicht Hören von den Menschen“

Immanuel Kant

1.1 Introduction

Although the quotation of Kant is disputatious, human ears are one of the most important organs of perception to process acoustic stimuli. Human hearing ability is important for communication and understanding each other. It delivers necessary information about dangerous situations and spatial surroundings and enables us to take part in a social life.
Technologies for assisted listening devices are desired to preserve natural hearing. For normal-hearing listeners, increasing listening comfort in complex acoustic scenes and achieving hearing protection are the most popular development scopes. For hearing impaired persons, assisted listening devices are crucial for better integration into our everyday life.

1.2 Motivation

In everyday environments, we are constantly surrounded by visual and acoustical stimuli. In these situations the human auditory system is able to concentrate on one source of interest (target source) while interfering sources are present. For normal-hearing listeners improvement in intelligibility is increased if the listener observes a spatial separation between target and interfering source [1], [2]. Localization cues are only available if the listener is presented with a binaural signal. The increased ability to hear signals in noise if the signal and noise have different perceived directions is referred to as spatial release from masking (SRM). Compared to normal-hearing listeners, hearing impaired persons have a higher speech reception threshold. This leads to a modified loudness perception and a reduced dynamic range. Consequently, acoustic events are separated badly and they can not benefit from SRM as much as normal-hearing persons.
Hearing aid algorithms aim at an improvement in intelligibility by performing on two main tasks: First, increasing signal-to-noise ratio (SNR) of the desired target source as noise reduction leads to an improvement in intelligibility. Second, preserving localisation cues to enhance spatial separation of sound sources, resulting again in an improvement in intelligibility.

1.3 Objective

The aim of this work is to improve speech intelligibility for hearing aid algorithms using differential microphone arrays (DMAs). The developed algorithm focuses on noise reduction as well as preserving localization cues. Microphone arrays and beamforming algorithms are very appropriate for noise reduction as they are supposed to enhance the target signal of one direction while suppressing interfering sources. One scenario is shown in Fig. 1.1a.

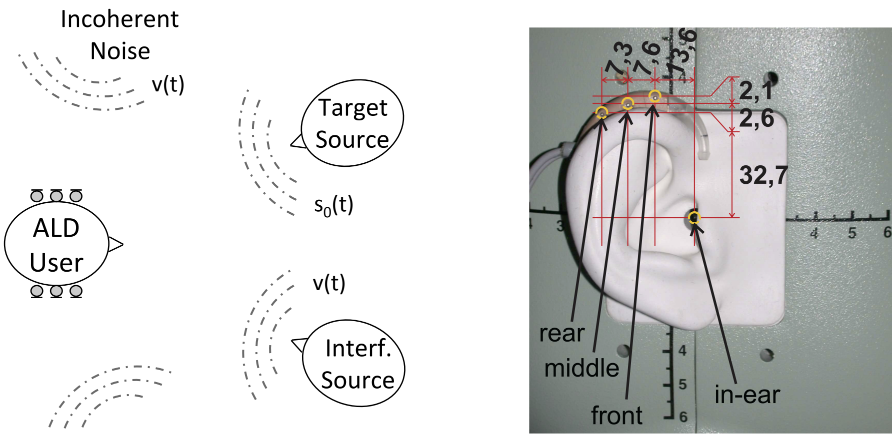

(a) (b)

Figure 1.1: (a) A scenario with one listener, one target source $s_0(t)$ and interfering sources $v(t)$, (b) schematic of the geometry of the microphones on the users head [3].

To preserve binaural cues a binaural signal presentation is needed. Binaural hearing aids share the information of both the left and the right hearing aid to generate an output for both ears. In contrast, monaural hearing aids processing only on its own microphone inputs to generate an output for its respective ear. A hearing impaired person wearing a monaural hearing aid on each ear is said to be using a bilateral hearing aid [4]. A comparison between a bilateral and a binaural hearing aid regarding speech intelligibility is given in the following chapters.
In this thesis a differential microphone array is used for beamforming algorithms. DMAs are suitable for hearing aids as they use a very compact arrangement. The beamforming algorithm of the DMA is adapted to the geometry of a hearing aid. A microphone setup of the hearing aid dummy which is used for the following calculations is shown in Fig. 1.1b.
All beamforming algorithms are implemented in MATLAB [5]. The analysis of the algorithms is based on calculated beampatterns and frequency responses. The evaluation is done by means of objective measures and an listening test.

1.4 Outline

This master's thesis is divided into the following chapters: The signal model used for all algorithms is described in chapter 2. Chapter 3 covers the fundamental concept of DMAs and the adapted applications for hearing aids. A fixed beamformer using all available microphones for a hearing aid geometry is presented in chapter 4. Chapter 5 focuses on different postfilter strategies while chapter 6 contains an evaluation between the discussed algorithms. An evaluation of a listening test is also presented in chapter 6. A detailed listing of the results is found in the appendix. Finishing with chapter 7 containing conclusion and outlook.

2 Fundamentals

Based on the fundamental concept of [6], the underlying signal model for this thesis is introduced. The notation is adopted and some measurements are presented. This algorithm defines the basis for the following chapters and further calculations.

2.1 Coordinate System

The model is based on a three-dimensional Cartesian coordinate system depicted in Fig. 2.1. The y-axis is perpendicular to the x-axis. Both axes span the xy-plane which is perpendicular to the z-axis. The centre of the coordinate system lies in the middle of the artificial head used for all simulations and described in Sec. 6.2. The x-axis points towards the target direction. Any position can be described by Cartesian coordinates $\{x,y,z\}$ or polar coordinates $\{r,\theta,\phi\}$.

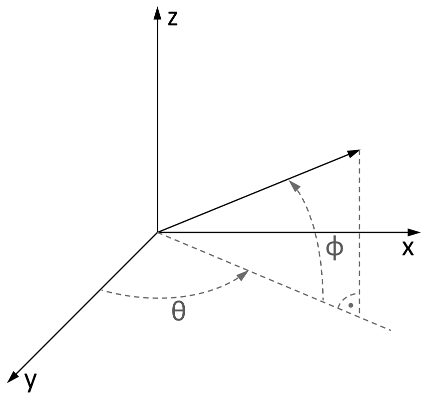

Figure 2.1: Three-dimensional Cartesian coordinate system.

2.2 Signal Model

The signal model is based on a uniform linear array (ULA) of M microphones depicted in Fig. 2.2.

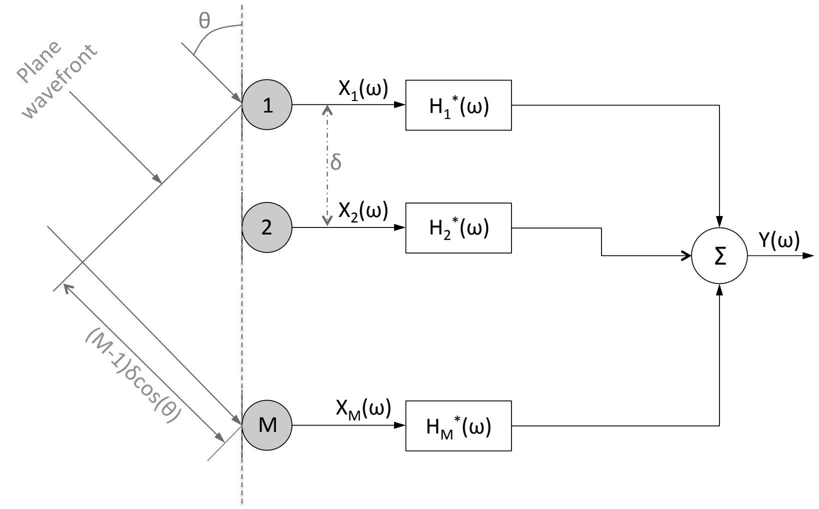

Figure 2.2: Schematic of a uniform linear array with processing filter $H_m(\omega)$ [6].

The array has equally spaced microphones with distance δ. The first microphone is taken as reference. Assuming one desired source signal, whose spherical wavefront impinges planar on the array, the time delay between the first and the mth acoustic sensor is given by

$$\tau_m = (m-1)\frac{\delta\cos(\theta)}{c}, \qquad m = 1, 2, \ldots, M \tag{2.1}$$

where m denotes the number of sensors, c is the propagation speed, i.e. $c = 343m/s$, and the angle θ describes the direction of the source signal impinging on the array. The time delay between two successive sensors at $\theta = 0°$ is

$$\tau_0 = \frac{\delta}{c} \tag{2.2}$$

The corresponding steering vector of length M taking all constraints into account is written by

$$\begin{aligned} \mathbf{d}(\omega,\theta) &= [1 \quad e^{-j\omega\delta_0/c\cos\theta} \quad \ldots \quad e^{-j(M-1)\omega\delta_M/c\cos\theta}]^T \\ &= [1 \quad (e^{-j\omega\tau_0\cos\theta})^1 \quad \ldots \quad (e^{-j\omega\tau_0\cos\theta})^{(M-1)}]^T \end{aligned} \tag{2.3}$$

where superscript ^{T} is the transpose operator, $j = \sqrt{-1}$ defines the imaginary unit, $\omega = 2\pi f$ is the angular frequency and $f > 0$ denotes the temporal frequency [6].

Assuming a single desired sound source impinging on the array, the received signal at discrete-time index k and the mth microphone can be written as

$$\begin{aligned} x_m(k) &= s_m(k) + v_m(k) \\ &= s(k - t - \tau_m) + v_m(k) \\ &= s(k - \tau_m) + v_m(k), \qquad m = 1, 2, \ldots, M, \quad t = 0 \end{aligned} \tag{2.4}$$

where t is the propagation time from the source $s(k)$ to microphone 1. The propagation time t will be neglected as this study only operates with relative time delays. Therefore, $s_m(k) = s(k - t - \tau_m) = s(k - \tau_m)$ and $v_m(k)$, respectively, are the signal of interest and noise signal observed at the mth microphone [6]. We assume that the noise signal $v_m(k)$ and source signal $s(k)$ are uncorrelated. For simplification of exposition Eq. (2.4) is rewritten in frequency domain. Taking the first microphone as reference, the mth microphone signal is given by

$$\begin{aligned} X_m(\omega) &= S_m(\omega) + V_m(\omega) \\ &= S(\omega)e^{-j\omega(t+\tau_m)} + V_m(\omega) \\ &= S(\omega)e^{-j(m-1)\omega\tau_0\cos\theta_s} + V_m(\omega), \qquad m = 1, 2, \ldots, M, \quad t = 0 \end{aligned} \tag{2.5}$$

where $S_m(\omega)$, $V_m(\omega)$ and $X_m(\omega)$ are the frequency-domain representations of $s_m(k)$,$v_m(k)$ and $x_m(k)$. Rewriting Eq. (2.5) in vector notation becomes

$$\begin{aligned}\mathbf{x}(\omega) &= [X_1(\omega) \quad X_2(\omega) \ \dots \ X_M(\omega)]^T \\ &= \mathbf{d}(\omega, \theta_s)S(\omega) + \mathbf{v}(\omega)\end{aligned} \tag{2.6}$$

with the noise vector defined as

$$\mathbf{v}(\omega) = [V_1(\omega) \quad V_2(\omega) \ \dots \ V_M(\omega)]^T \ . \tag{2.7}$$

As shown in Fig. 2.2 a filter weight $H_m(\omega, \theta_s)$ is applied at the output of each microphone. The beamformer output of the ULA for an angular frequency ω at target direction θ_s is then

$$\begin{aligned}Y(\omega) &= \sum_{m=1}^{M} H_m^*(\omega, \theta_s)X_m(\omega) \\ &= \mathbf{h}^H(\omega, \theta_s)\mathbf{x}(\omega) \\ &= \mathbf{h}^H(\omega, \theta_s)\mathbf{d}(\omega, \theta_s)S(\omega) + \mathbf{h}^H(\omega, \theta_s)\mathbf{v}(\omega)\end{aligned} \tag{2.8}$$

where superscripts * and ^{H} denote complex conjugation and conjugate-transpose operator. As mentioned in Sec. 2.1 the x-axis points towards the source direction. This leads to $\theta_s = 0°$ following $\cos\theta_s = 1$. The beamforming filter of length M is rewritten as

$$\mathbf{h}(\omega) = [H_1(\omega) \quad H_2(\omega) \ \dots \ H_M(\omega)]^T \tag{2.9}$$

where superscript ^{T} is the transpose operator.

2.3 Beampattern

The sensitivity of each beamformer varies according to the direction the sound is arriving from. The beampattern describes the sensitivity of the beamformer to a plane wave impinging on the array from direction θ. It is defined as the magnitude of the transfer function between the beamformer output and input signal.

$$\begin{aligned}\mathcal{B}(\omega, \theta_s, \theta) &= \left| \frac{X(\omega, \theta)}{S(\omega)} \right| \\ &= \mathbf{d}^H(\omega, \theta)\mathbf{h}(\omega, \theta_s) \\ &= \sum_{m=1}^{M} \mathbf{H}_m(\omega, \theta_s)e^{j(m-1)\omega\tau_0 \cos\theta}\end{aligned} \tag{2.10}$$

Directivity Factor and Directivity Index

The directivity factor of an Nth order DMA is defined as the ratio between the directivity pattern at direction $\theta = \theta_s$ and the averaged directivity pattern over the whole space.

$$\mathcal{G}_N(\theta) = \frac{\mathcal{B}_N^2(0)}{\frac{1}{\pi}\displaystyle\int_{\theta_s}^{\theta_s+\pi} \mathcal{B}_N^2(\theta - \theta_s)d\theta} \tag{2.11}$$

The Directivity index is defined as

$$\mathcal{D}_N(\theta) = 10\log_{10}\mathcal{G}_N(\theta) \tag{2.12}$$

3 Differential Microphone Array

This chapter introduces a formulation of a differential microphone arrays design problem. It discusses several basic mathematical concepts and reveals the basic properties. Furthermore, an adaptive version of differential microphone arrays is discussed. Considering the hearing aid geometry described in Sec. 1.3, the calculations are adapted to this specific geometry.

3.1 Introduction

The main idea of microphone arrays is to extract a desired speech signal out of a noisy environment and interfering sources by sampling the sound field with spatial diversity. How well the signal enhancement is accomplished is conditioned on a number of factors, i.e. number of sensors, array geometry and processing algorithm. Based on additive microphone arrays the main principle is to add the sensors output in such a way that the signal of interest is extracted while noise and interference is suppressed. Although an optimal gain in steering direction is achieved, the main lobe is frequency-dependent and a lot of side lobes are produced due to spatial aliasing. In contrast to additive microphone arrays, differential microphone arrays respond to the spatial derivatives of the acoustic pressure field. This means a directional pattern is formed by measuring the differentials of the acoustic pressure field between a number of omnidirectional sensors. An Nth-order differential is formed by subtracting two differentials of order $N-1$. The response of a Nth-order DMA is proportional to a linear combination of signals derived from spatial derivatives from order 0 to N. Hence, the microphone distance δ must be small enough so that the true acoustic pressure differential can be approximated. Avoiding spatial aliasing, it is assumed that the distance δ is much smaller than the acoustic wavelength $\lambda = \frac{c}{f}$.
Holding $\delta \ll \lambda$ implies that

$$\frac{\omega\delta}{c} = \omega\tau_0 \ll 2\pi \tag{3.1}$$

For optimal performance a DMA is used in endfire direction ($\theta = 0°$). According to Sec. 2.1 the main-steering direction and the desired signal propagate at the same angle $\theta = \theta_s = 0°$.
The fundamental difference between additive and differential microphone arrays is the conception of the beamforming filter. In additive arrays the filter elements are optimized to steer the main lobe in the direction of the desired signal, whereas in differential microphone arrays the filter is optimized to steer a certain number of nulls in a specific direction. Especially the small array

aperture and the frequency-independent beampattern are optimal for the use in hearing aids. Summarizing, differential microphone arrays have the following advantages and disadvantages:

Advantages

- frequency-invariant beampattern (more suitable for broadband signals, like speech signals)
- effective at high and low frequencies
- potential to attain maximum directional gain for a given number of sensors
- compact microphone array aperture

Disadvantages

- high-pass filter with a slope of $6N$ dB/octave (frequency response has to be properly compensated)
- frequency response and level depends on the position and orientation of the array relative to the sound source
- suffering of white noise amplification due to the compensation filter particular at low frequencies

3.2 First-Order Differential Microphone Array

A first-order DMA is designed with $M = 2$ microphones. In this approach two constraints have to be fulfilled. First, distortionless response, resulting in a gain of one, has to be achieved at the angle of $\theta = 0°$ (endfire direction). Second, a null is steered within the interval of $90° \leq \theta_{1,1} \leq 180°$. The filter elements are obtained by solving a set of M linear equations

$$\mathbf{d}^H(\omega, \cos 0°)\mathbf{h}(\omega) = \mathbf{d}^H(\omega, 1)\mathbf{h}(\omega) = 1 \tag{3.2}$$

$$\mathbf{d}^H(\omega, \alpha_{1,1})\mathbf{h}(\omega) = \beta_{1,1} \tag{3.3}$$

where $\beta_{1,1} = 0$ and $\alpha_{1,1} = \cos\theta_{1,1}$ is given by design with $-1 \leq \alpha_{1,1} \leq 0$. The location of the steered null corresponds to the angle $\theta_{1,1}$ in the beampattern. In matrix notation Eq. (3.2) and Eq. (3.3) can be expressed as

$$\begin{bmatrix} \mathbf{d}^H(\omega, 1) \\ \mathbf{d}^H(\omega, \alpha_{1,1}) \end{bmatrix} \mathbf{h}(\omega) = \begin{bmatrix} 1 \\ 0 \end{bmatrix} \tag{3.4}$$

Rewriting Eq. (3.4) with specific values for $\theta = 0°$ and $\alpha_{1,1} = \cos\theta_{1,1}$, it is

$$\begin{bmatrix} 1 & e^{j\omega\tau_0} \\ 1 & e^{j\omega\tau_0\alpha_{1,1}} \end{bmatrix} \mathbf{h}(\omega) = \begin{bmatrix} 1 \\ 0 \end{bmatrix} \tag{3.5}$$

Solving Eq. (3.5) for $\mathbf{h}(\omega)$ a first-order DMA filter is designed:

$$\mathbf{h}(\omega) = \frac{1}{1 - e^{j\omega\tau_0(1-\alpha_{1,1})}} \begin{bmatrix} 1 \\ -e^{-j\omega\tau_0\alpha_{1,1}} \end{bmatrix} \tag{3.6}$$

As the sensor spacing is much smaller than the acoustic wavelength, the plane wave assumption holds and the approximation $e^x \approx 1 + x$ can be used in Eq. (3.6). This leads to

$$\mathbf{h}(\omega) \approx \frac{j}{(1-\alpha_{1,1})\tau_0\omega} \begin{bmatrix} 1 \\ -e^{-j\omega\tau_0\alpha_{1,1}} \end{bmatrix} = H_L(\omega) \begin{bmatrix} H_1(\omega) \\ H_2(\omega) \end{bmatrix} \tag{3.7}$$

By separating the beamforming filter $\mathbf{h}(\omega)$ into a low-pass filter $H_L(\omega)$ and two filter element gains $H_1(\omega)$ and $H_2(\omega)$, a more common structure is obtained shown in Fig. 3.1a. The filter element gains are applied at the two microphone outputs according to Fig. 2.2.

$$\begin{aligned} H_1(\omega) &= 1 \\ H_2(\omega) &= -e^{-j\omega\tau_0\alpha_{1,1}} \\ H_L(\omega) &= \frac{j}{(1-\alpha_{1,1})\tau_0\omega} \end{aligned} \tag{3.8}$$

The calculation of the first-order beampattern leads to

$$\begin{aligned} \mathcal{B}(\omega,\theta_s,\theta) &= \mathbf{d}^H(\omega,\theta)\mathbf{h}(\omega) \\ &= \frac{j}{(1-\alpha_{1,1})\tau_0\omega}(1-e^{-j\omega\tau_0(\cos\theta-\alpha_{1,1})}) \end{aligned} \tag{3.9}$$

Again the approximation $e^x \approx 1+x$ is used in Eq. 3.9 resulting in a frequency-independent beampattern:

$$\mathcal{B}(\omega,\theta) = \frac{1}{(1-\alpha_{1,1})}(\cos\theta-\alpha_{1,1}) \tag{3.10}$$

Different beampatterns, as depicted in Fig. 3.1b, are generated by the use of different $\alpha_{1,1}$. The values of $\alpha_{1,1}$ for the following beampatterns are:

- Dipole: $\theta_{1,1} = 90°$ corresponds to $\alpha_{1,1} = 0$
- Cardioid: $\theta_{1,1} = 180°$ corresponds to $\alpha_{1,1} = -1$
- Hypercardioid: $\theta_{1,1} = 120°$ corresponds to $\alpha_{1,1} = -\frac{1}{2}$
- Supercardioid: $\theta_{1,1} = 135°$ corresponds to $\alpha_{1,1} = -\frac{1}{\sqrt{2}}$

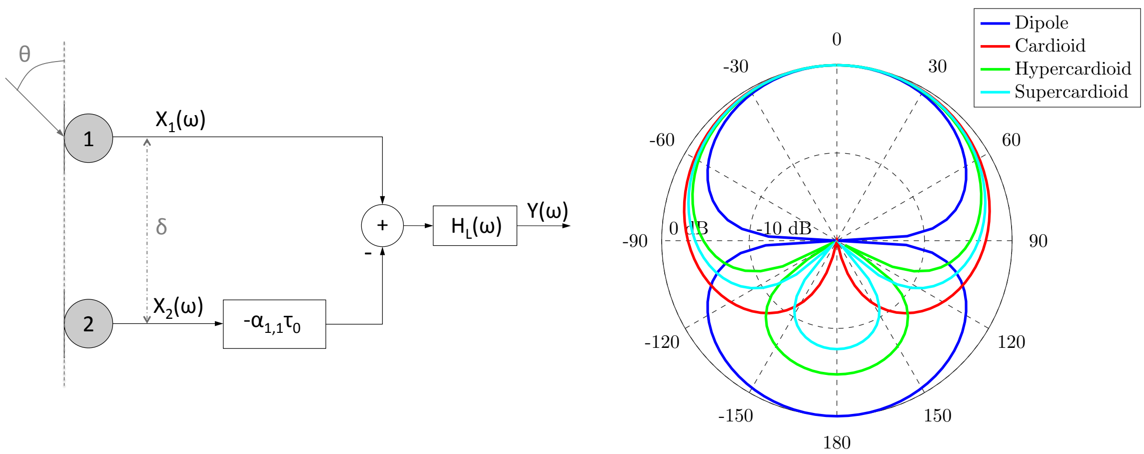

(a) (b)

Figure 3.1: First-order DMA: (a) common structure [7], (b) different beampatterns for $f = 1000Hz$.

3.2.1 Compensation Filter $H_L(\omega)$

In Fig. 3.2a the directional response of a first-order DMA for a target direction $\theta = 0$ is shown. The frequency-dependence has to be compensated up to a certain cut-off frequency. The cut-off frequency is dependent on the microphone distance δ as $\delta \stackrel{!}{=} \frac{\lambda}{4}$ to avoid spatial aliasing. This leads to

$$\omega_c = \frac{\pi}{2\tau_0} \tag{3.11}$$

An ideal compensation filter proposed in [8] is then

$$H_{L_{id}}(\omega) = \begin{cases} \frac{1}{2\sin(\frac{\pi}{2}\frac{\omega}{\omega_c})} & , 0 < \omega < \omega_c \\ \frac{1}{2} & , otherwise \end{cases} \tag{3.12}$$

3.2.2 Frequency Response of First-Order DMA

For different angle of incidence, the frequency response of a first-order cardioid is shown in Fig. 3.2. The sensor spacing is $\delta \approx 0.008m$. Fig. 3.2a depicts the directional response without compensation filter $H_L(\omega)$. The high-pass characteristic with a slope of approximately 6 db/octave in the low frequency range of $f < 4000Hz$ is clearly visible. Distinctive notches are characteristic at high frequency range. Although the frequency response is linear in the low frequency range, it is frequency-dependent without a compensation filter.
Fig. 3.2b shows the frequency response with compensation filter $H_L(\omega)$. It is obvious that the directional characteristic gets frequency-independent due to the compensation filter. It is clearly understood that the amplification of low frequencies entails the amplification of uncorrelated white noise, e.g. like sensor noise. The White Noise Gain (WNG) is dependent on the characteristic of the compensation filter. To reduce WNG, a larger sensor spacing δ is appropriate. This contradicts the constraint for DMAs, which claims a small δ. Hence, there is always a trade-off between white noise amplification and a frequency-independent beampattern.
Fig. 3.2c shows the directional response with the ideal compensation filter $H_{L_{id}}(\omega)$ proposed in Eq. (3.12). The frequency response is compensated up to a certain cut-off frequency (red marked in Fig. 3.2a). For lower frequencies the compensation is the same as in Fig. 3.2b whereas for higher frequencies the notches are not suppressed. The following plots are plotted with a sampling frequency of $f_s = 48kHz$. For this example, the notches at higher frequencies are irrelevant as they lie already above the Nyquist-frequency $f_N = f_s/2$.

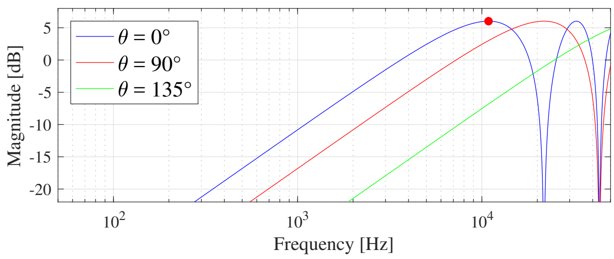

(a)

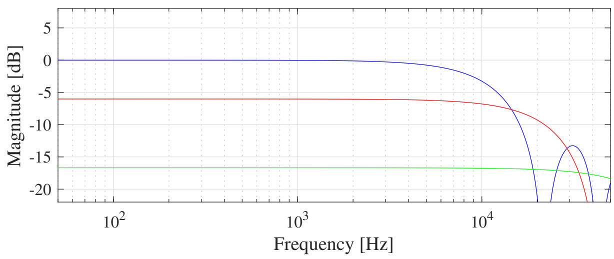

(b)

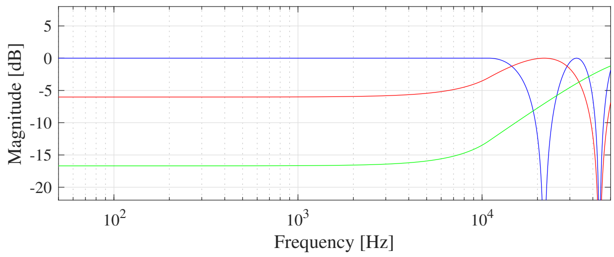

(c)

Figure 3.2: Frequency response of a first-order DMA with sensor spacing $\delta \approx 0.008m$: (a) without compensation filter, (b) with compensation filter, (c) with ideal compensation filter.

3.3 Second-Order Differential Microphone Array for Hearing Aids

The second-order DMA is generated out of the first-order by increasing the number of acoustic sensors. An array of $M = 3$ microphone is needed. To use a second-order DMA in a hearing aid proposed in Sec. 1.3 the calculations have to be adapted to the geometry. Precisely, the time delays of two successive sensors must be adapted as the distance between the microphones is not equal to each other. A common structure with unequally spaced microphones is depicted in Fig. 3.3a. The steering vector for a second-order DMA changes to

$$\mathbf{d}(\omega, \theta) = [1 \quad e^{-j\omega\tau_0 \cos\theta} \quad e^{-j\omega(\tau_0+\tau_1)\cos\theta}]^T \tag{3.13}$$

with $\tau_0 = \delta_0/c$ and $\tau_1 = \delta_1/c$. For a second-order DMA three constraints have to be fulfilled. First, a one is steered at the angle of $\theta = 0°$, Second, two nulls are steered within the interval of $0° < \theta_{2,n} \leq 180°$. In matrix notation it is written as

$$\begin{bmatrix} \mathbf{d}^H(\omega, 1) \\ \mathbf{d}^H(\omega, \alpha_{2,1}) \\ \mathbf{d}^H(\omega, \alpha_{2,2}) \end{bmatrix} \mathbf{h}(\omega) = \begin{bmatrix} 1 \\ \beta_{2,1} \\ \beta_{2,2} \end{bmatrix} \tag{3.14}$$

with $\alpha_{2,1} = \cos\theta_{2,1}$ and $\alpha_{2,2} = \cos\theta_{2,2}$ are given by design with $-1 \leq \alpha_{2,1} < 1$, $-1 \leq \alpha_{2,2} < 1$ and $\alpha_{2,1} \neq \alpha_{2,2}$. $\beta_{2,1}$ and $\beta_{2,2}$ have to be in the range of $0 \leq \beta_{2,1} \leq 1$ and $0 \leq \beta_{2,2} \leq 1$. Here, only the assumption for two distinct nulls in different directions is presented, meaning $\beta_{2,1} = \beta_{2,2} = 0$. Rewriting Eq. (3.14) to

$$\begin{bmatrix} 1 & e^{j\omega\tau_0} & e^{j\omega(\tau_0+\tau_1)} \\ 1 & e^{j\omega\tau_0\alpha_{2,1}} & e^{j\omega(\tau_0+\tau_1)\alpha_{2,1}} \\ 1 & e^{j\omega\tau_0\alpha_{2,2}} & e^{j\omega(\tau_0+\tau_1)\alpha_{2,2}} \end{bmatrix} \mathbf{h}(\omega) = \begin{bmatrix} 1 \\ 0 \\ 0 \end{bmatrix} \tag{3.15}$$

and solving for $\mathbf{h}(\omega)$ leads to

$$\mathbf{h}(\omega) = H_L(\omega) \begin{bmatrix} H_1(\omega) \\ H_2(\omega) \\ H_3(\omega) \end{bmatrix} \tag{3.16}$$

$$H_1(\omega) = e^{j\omega\tau_0(\alpha_{2,1}+\alpha_{2,2})}(e^{j\omega\tau_1\alpha_{2,1}} - e^{j\omega\tau_1\alpha_{2,2}}) \tag{3.17}$$

$$H_2(\omega) = (e^{j\omega(\tau_0+\tau_1)\alpha_{2,2}} - e^{j\omega(\tau_0+\tau_1)\alpha_{2,1}}) \tag{3.18}$$

$$H_3(\omega) = (e^{j\omega\tau_0\alpha_{2,1}} - e^{j\omega\tau_0\alpha_{2,2}}) \tag{3.19}$$

$$H_L(\omega) = \frac{1}{\substack{(e^{j\omega(\tau_0+\tau_1)} - e^{j\omega(\tau_0+\tau_1)\alpha_{2,2}})(e^{j\omega\tau_0\alpha_{2,1}} - e^{j\omega\tau_0\alpha_{2,2}})\cdots \\ \cdots - (e^{j\omega(\tau_0+\tau_1)\alpha_{2,1}} - e^{j\omega(\tau_0+\tau_1)\alpha_{2,2}})(e^{j\omega\tau_0} - e^{j\omega\tau_0\alpha_{2,2}})}} \tag{3.20}$$

Again, the second-order beampattern is calculated as

$$\mathcal{B}(\omega,\theta_s,\theta) = \mathbf{d}^H(\omega,\theta)\mathbf{h}(\omega)$$
$$= \begin{bmatrix}1 & e^{j\omega\tau_0\cos\theta} & e^{j\omega(\tau_0+\tau_1)\cos\theta}\end{bmatrix} \begin{bmatrix} e^{j\omega\tau_0(\alpha_{2,1}+\alpha_{2,2})}\left(e^{j\omega\tau_1\alpha_{2,1}} - e^{j\omega\tau_1\alpha_{2,2}}\right) \\ e^{j\omega(\tau_0+\tau_1)\alpha_{2,2}} - e^{j\omega(\tau_0+\tau_1)\alpha_{2,1}} \\ e^{j\omega\tau_0\alpha_{2,1}} - e^{j\omega\tau_0\alpha_{2,2}} \end{bmatrix} H_L(\omega) \tag{3.21}$$

The variation of $\alpha_{2,1}$ and $\alpha_{2,2}$ results in different beampatterns depicted in Fig. 3.3b. There has not been observed any difference of the beampatterns between equally or unequally spaced microphones. The values of $\alpha_{2,1}$ and $\alpha_{2,2}$, which have been used for the following beampatterns are:

- Cardioid: $\alpha_{2,1} = \frac{1}{2}$, $\alpha_{2,2} = -1$
- Hypercardioid: $\alpha_{2,1} = -0.81$, $\alpha_{2,2} = 0.31$
- Quadrupol: $\alpha_{2,1} = -\frac{1}{\sqrt{2}}$, $\alpha_{2,2} = \frac{1}{\sqrt{2}}$

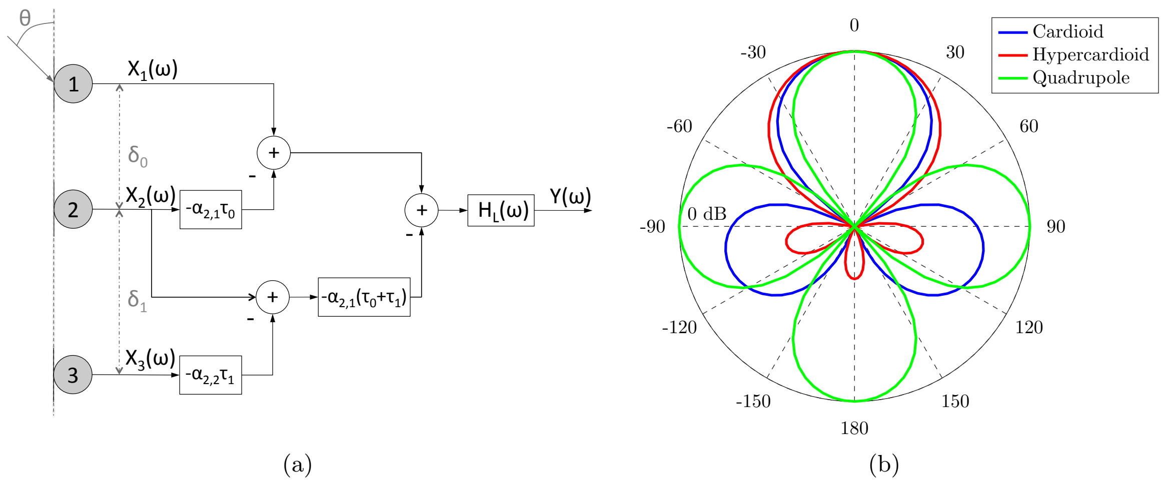

Figure 3.3: Second-order DMA: (a) common structure, (b) different beampatterns for $f = 1000Hz$.

3.3.1 Frequency Response of Second-Order DMA

The frequency response of a second-order DMA adapted to the geometry of a hearing aid is shown in Fig. 3.4. The high-pass characteristic with a distinctive slope of 12 dB/octave is clearly visible in Fig. 3.4a.
Using the compensation filter calculated in Sec. 3.3 the directional characteristic gets frequency-independent as depicted in 3.4b. The compensation filter is only applied up to a certain cut-off frequency (red marked) to circumvent the amplification of higher frequencies $f > 14kHz$. This would lead to a highly non-linear frequency response.

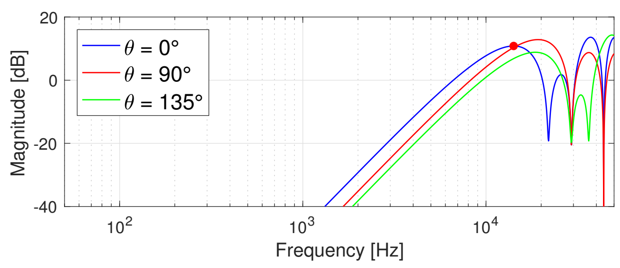

(a)

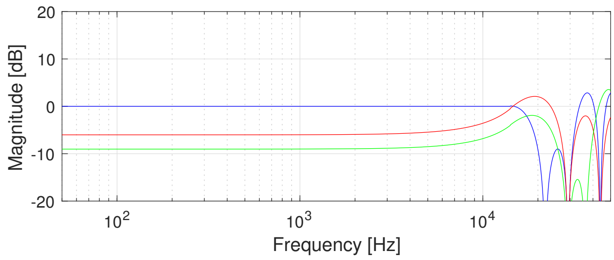

(b)

Figure 3.4: Frequency response of a second-order DMA with sensor spacing $\delta \approx 0.008m$: (a) without compensation filter, (b) with compensation filter

3.4 Adaptive First-Order Differential Microphone Array

In real situations a variable beampattern is needed to form a distinctive null in the rear half plane. One simple implementation would be an adjustable time delay τ_0 to form a first-order adaptive DMA. For this solution the computational effort is very high and therefore not attractive for real-time implementations. A better way is to form a back-to-back cardioid arrangement. This means, a fixed forward-facing cardioid and a fixed backward-facing cardioid are generated by a fixed beamformer (cf. Sec. 3.2). Both cardioids are then combined to form an overall output. The adaptive algorithm aims at minimizing the microphone output power under the constraint that the null is located in the rear-half plane [7].
Recalling Sec. 3.2, the fixed beamformer outputs forming a forward-facing cardioid $C_f(\omega, \theta)$ and a backward-facing cardioid $C_b(\omega, \theta)$ are generated by

$$C_f(\omega, \theta) = \begin{bmatrix} 1 & e^{-j\omega\tau_0 \cos\theta} \end{bmatrix} \begin{bmatrix} 1 \\ -e^{-j\omega\tau_0} \end{bmatrix} S(\omega) \tag{3.22}$$

$$C_b(\omega, \theta) = \begin{bmatrix} 1 & e^{-j\omega\tau_0 \cos\theta} \end{bmatrix} \begin{bmatrix} -e^{-j\omega\tau_0} \\ 1 \end{bmatrix} S(\omega) \tag{3.23}$$

The following Fig. 3.5 shows the schematic implementation of a first-order ADMA.

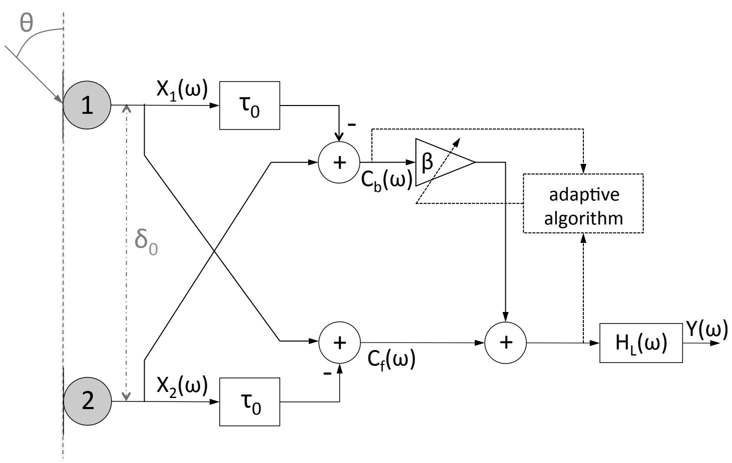

Figure 3.5: Schematic of a first-order adaptive differential microphone array [7].

The overall output signal normalized by the input spectrum $S(\omega)$ is calculated by (cf. Fig. 3.5)

$$\begin{aligned}\left|\frac{Y(\omega,\theta)}{S(\omega)}\right| &= |(C_f(\omega,\theta) - \beta C_b(\omega,\theta))H_L(\omega)| \\ &= \left| \begin{bmatrix}1 & e^{-j\omega\tau_0\cos\theta}\end{bmatrix} \begin{bmatrix}1 \\ -e^{-j\omega\tau_0}\end{bmatrix} - \beta \begin{bmatrix}1 & e^{-j\omega\tau_0\cos\theta}\end{bmatrix} \begin{bmatrix}-e^{-j\omega\tau_0} \\ 1\end{bmatrix} H_L(\omega)\right|\end{aligned} \tag{3.24}$$

3.4.1 Optimum β

The optimum β minimizes the mean-square value of the sensor output $y(t)$. According to [7], the output of the back-to-back cardioid in time-domain is

$$y(t) = c_f(t) - \beta c_b(t) \tag{3.25}$$

Squaring the output and taking the expected value yields to

$$E[y^2(t)] = P_{c_f c_f}(0) - 2\beta P_{c_f c_b}(0) + \beta^2 P_{c_b c_b}(0) \tag{3.26}$$

where $P_{c_f c_f}(0)$ and $P_{c_b c_b}(0)$ are the powers of the front- and backward-cardioid signals and $P_{c_f c_b}(0)$ is the cross-power between those signals. The minimum value can be found by taking the derivative of Eq. (3.26) with respect to β and setting the result to zero. The optimum value corresponds to an optimum Wiener filter of filter length one and is calculated by

$$\beta_{opt} = \frac{P_{c_f c_b}(0)}{P_{c_b c_b}(0)} \tag{3.27}$$

3.4.2 Normalized Least Mean Square (NLMS)

The LMS algorithm is commonly used for real-time implementations due to its simplicity and low computational effort [9]. The advantage of the NLMS algorithm in contrast to the LMS algorithm is the adaptation of the step-size μ according to the current input power. The step-size μ is written to

$$\mu = \frac{\mu_0}{\|c_b^2(t)\| + \Delta}, \quad 0 < \mu_0 < 2 \tag{3.28}$$

where Δ is a regularization parameter to prevent large μ's. The NLMS algorithm for the back-to-back cardioid arrangement of an adaptive first-order differential array is then

$$\begin{aligned}\beta_{t+1} &= \beta_t + \mu y(t) c_b(t) \\ &= \beta_t + \mu_0 \frac{y(t) c_b(t)}{\|c_b^2(t)\| + \Delta}\end{aligned} \tag{3.29}$$

Fig. 3.6a shows the forward-facing cardioid and backward-facing cardioid according to Eq. (3.22) and Eq. (3.23). The created beampatterns with different β are depicted in Fig. 3.6b. The values of β which have been used for the following beampatterns are:

- Dipole: $\beta = 1$
- Cardioid: $\beta = 0$
- Hypercardioid: $\beta = 0.172$

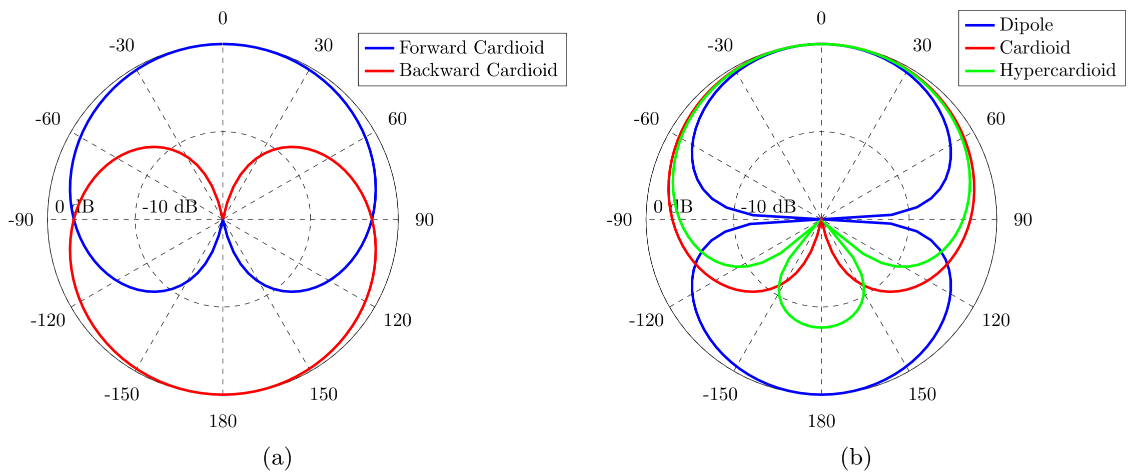

Figure 3.6: Beampatterns of first-order ADMA: (a) forward- and backward-facing cardioid, (b) different beampattern for $f = 1000Hz$.

3.5 Adaptive Second-Order Differential Array for Hearing Aids

The second-order ADMA is an extension of the first-order ADMA and is able to suppress two interfering sources. The processing structure is essentially the same as for a first-order ADMA and is shown in Fig. 3.7. A fixed beamformer is used to form three base-beampatterns, a forward cardioid $C_{ff}(\omega, \theta)$, a backward cardioid $C_{bb}(\omega, \theta)$ and a toroid $C_{tt}(\omega, \theta)$. These base-beampatterns form the input for the adaptive beamformer. The overall output is generated adaptively by a weighted sum of these three base-beampatterns.

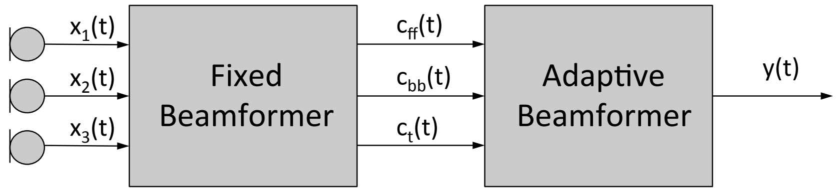

Figure 3.7: Block diagram of second-order adaptive differential microphone array [10].

To use a second-order ADMA in the proposed hearing aid, the fixed beamformer has to be adapted. As the distance between the microphones is not equal, different time delays are needed. The schematic structure of the fixed beamformer stage is shown in Fig. 3.8.

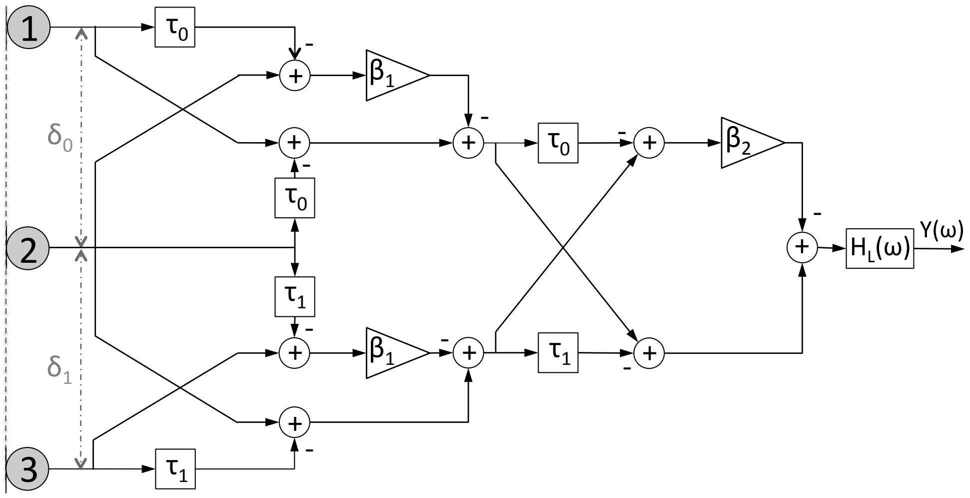

Figure 3.8: Schematic implementation of an adaptive second-order differential array using fixed delay elements but different sensor spacings δ.

The second-order ADMA can be seen as a cascade of a first-order back-to-back cardioid arrangement using fixed time delay elements. Using different values of β the forward-facing cardioid $C_{ff}(\omega,\theta)$, backward-facing cardioid $C_{bb}(\omega,\theta)$ and toroid $C_{tt}(\omega,\theta)$, can be written as

$$C_{ff}(\omega,\theta) = \begin{bmatrix}1 & e^{-j\omega\tau_0\cos\theta} & e^{-j\omega(\tau_0+\tau_1)\cos\theta}\end{bmatrix} \begin{bmatrix}1 \\ -e^{-j\omega\tau_0} - e^{-j\omega\tau_1} \\ e^{-j\omega 2\tau_1}\end{bmatrix} S(\omega) \tag{3.30}$$

$$C_{bb}(\omega,\theta) = \begin{bmatrix}1 & e^{-j\omega\tau_0\cos\theta} & e^{-j\omega(\tau_0+\tau_1)\cos\theta}\end{bmatrix} \begin{bmatrix}e^{-j\omega 2\tau_0} \\ -e^{-j\omega\tau_0} - e^{-j\omega\tau_1} \\ 1\end{bmatrix} S(\omega) \tag{3.31}$$

$$C_{tt}(\omega,\theta) = \begin{bmatrix}1 & e^{-j\omega\tau_0\cos\theta} & e^{-j\omega(\tau_0+\tau_1)\cos\theta}\end{bmatrix} \begin{bmatrix}-2e^{-j\omega\tau_0} \\ 2 + e^{-j\omega 2\tau_0} + e^{-j\omega 2\tau_1} \\ -2e^{-j\omega\tau_1}\end{bmatrix} S(\omega) \tag{3.32}$$

The adaptive beamformer stage is depicted in Fig. 3.9. The weighting of the base-beampatterns is achieved by the adaptive gains α_n.

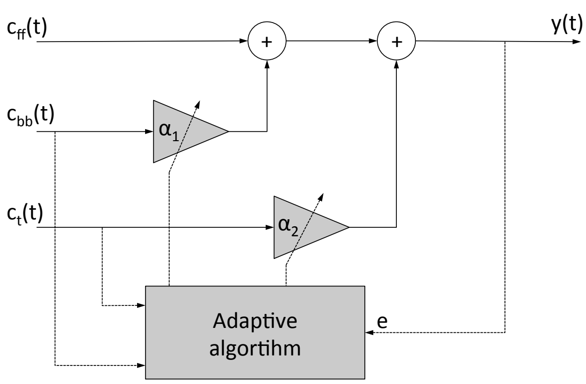

Figure 3.9: Block diagram of second-order adaptive beamformer [10].

The overall output signal $Y(\omega,\theta)$ is calculated by (cf. Fig. 3.9)

$$\left|\frac{Y(\omega,\theta)}{S(\omega)}\right| = |(C_{ff}(\omega,\theta) - \alpha_1 C_{bb}(\omega,\theta) - \alpha_2 C_{tt}(\omega,\theta))H_L(\omega)| \tag{3.33}$$

3.5.1 Optimum α

A NLMS algorithm is applied to the three base-beamformed signals according to [10]. The error signal, which is the same as the output signal $y(t)$ of the beamformer, is computed according to

$$e = c_{ff} - \alpha^T c \tag{3.34}$$

where

$$\alpha = \begin{bmatrix}\alpha_1(t) & \alpha_2(t)\end{bmatrix}^T \tag{3.35}$$

and

$$c = \begin{bmatrix}c_{bb}(t) & c_{tt}(t)\end{bmatrix}^T \tag{3.36}$$

The optimum α is now calculated by an NLMS algorithm

$$\alpha_{t+1} = \alpha_t + \mu \frac{e(t)\mathbf{c}(t)}{\|\mathbf{c}(\mathbf{t})^2\| + \Delta} \tag{3.37}$$

with the step-size μ and the regularization parameter Δ. To limit the position of the zeros in the beampattern, a constraint to α is necessary. By limiting α to $-1 \leq \alpha_{1,2} \leq 1$, the zeros in the beampattern are limited to the rear half plane within the angle $90° \leq \theta \leq 270°$. Fig. 3.10a shows the forward-facing cardioid, backward-facing cardioid and toroid according to Eq. (3.30), (3.31) and (3.32). The created beampatterns with different α_n are depicted in Fig. 3.10b. The values of α_n for the following beampatterns are:

- Dipole: $\alpha_1 = 1$ and $\alpha_2 = 0$
- Cardioid: $\alpha_1 = 0$ and $\alpha_2 = 1$
- Hypercardioid: $\alpha_1 = 0$ and $\alpha_2 = 0$

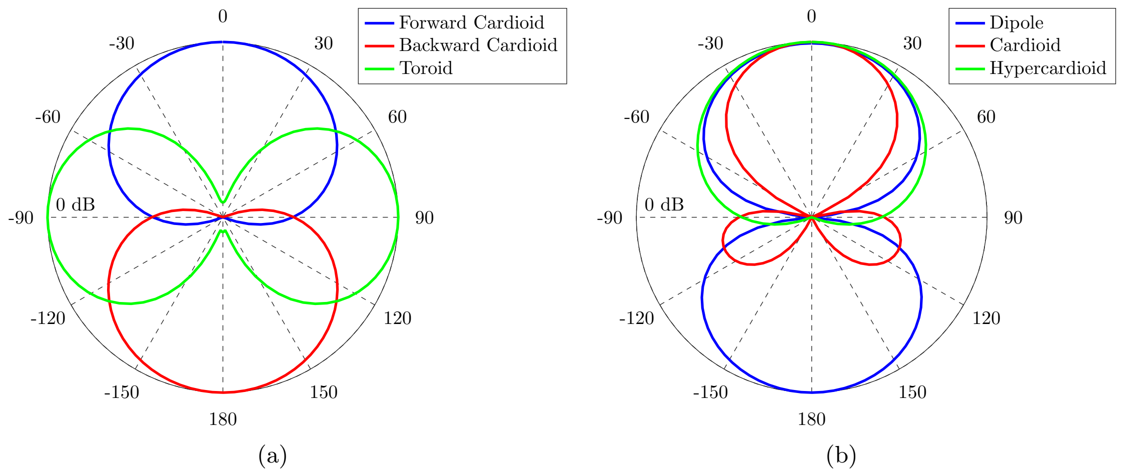

Figure 3.10: Beampatterns of second-order ADMA: (a) cardioids of second-order ADMA, (b) different beampatterns for $f = 1000Hz$

3.6 Hybrid Structure

Frequency Dependence f_{Hyb}

The main problem of the second-order DMA is the large amplification of uncorrelated white noise. This makes an implementation for real situations not useful. To avoid the large amplification a hybrid structure can be used. This means, a first-order ADMA is used at low frequency range and a second-order ADMA is used at high frequency range. The hybrid structure is shown in Fig. 3.11.

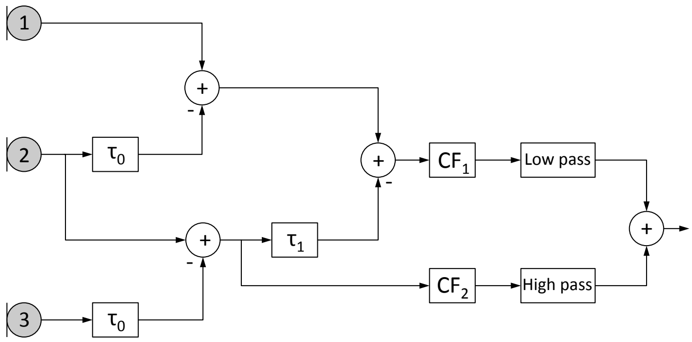

Figure 3.11: Schematic implementation of hybrid structure using first- and second-order ADMA [11].

Figure 3.12 depicts the frequency response of the hybrid structure for low- and high-pass filter. The cut-off frequency depends on the WNG. In this example a cut-off frequency of $f = 1000Hz$ is used at which the normalized gain of the filter is -6dB.

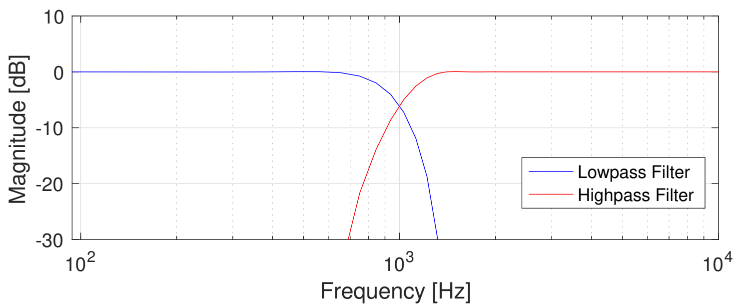

Figure 3.12: Low- and high-pass filter for hybrid structure.

Level Dependence L_{Hyb}

Another method to avoid the amplification of uncorrelated white noise is to make the directivity dependent on the input level rather than the frequency (cf. Sec. 3.6). At low input level, a beamformer is not needed and the input of the reference microphone (i.e. first microphone) can directly be connected to the output. If the level increases more directivity is needed and a first- or second-order ADMA is applied. The decision for the first- or second-order ADMA is dependent on the signal-to-noise ratio. At high SNR, only a first-order beamformer is used, otherwise a second-order beamformer is applied. The amplification of white noise is not as much taken into account for high levels than for low levels as it is masked to a large extend with the input signal. In Fig. 3.13 the decision boundaries are depicted schematically.

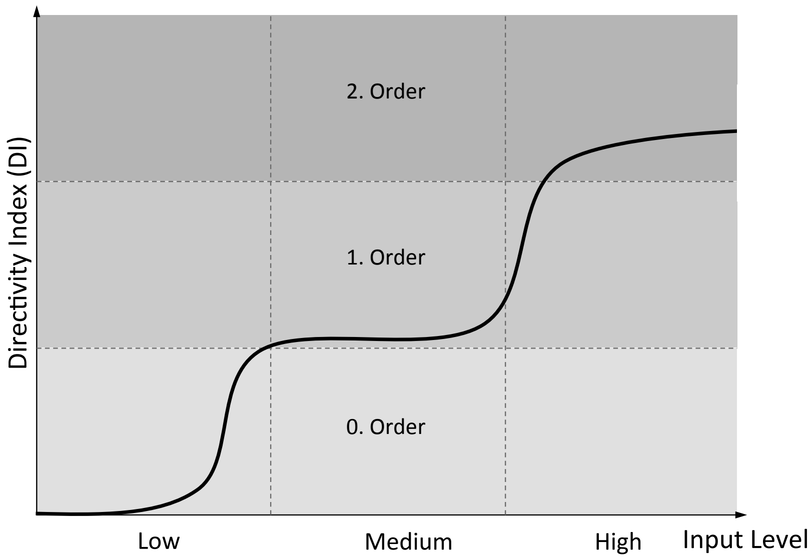

Figure 3.13: Principle of the input level dependent directivity [11].

4

Fixed Beamformer for Hearing Aid Geometry

This chapter gives an overview of the design of circular differential microphone arrays according to [12]. Based on this design a beamforming algorithm for hearing aids using six microphones is developed. The first- and the second-order are discussed and the main properties are revealed.

4.1 Introduction to Circular Differential Microphone Array

In Fig. 4.1 a schematic of a uniform circular array (UCA) is depicted.

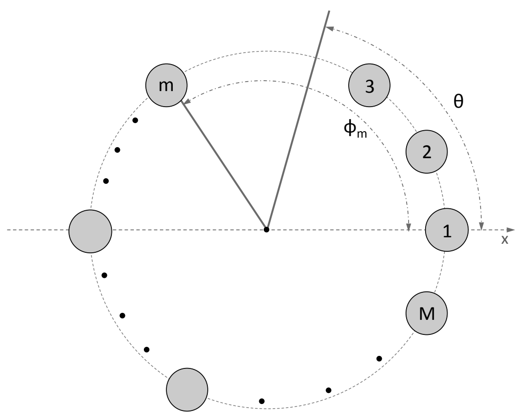

Figure 4.1: Schematic of a circular differential array [12].

The time delay is calculated between the mth microphone and the origin of the array. It is assumed that the origin of the array coincides with the origin of the Cartesian coordinate system. Sensor 1 is placed on the x-axis of the coordinate system. The angle θ describes the direction of the source signal impinging on the array. It is supposed that a wavefront impinges planar on the array as the distance δ between the sensors is small compared to the wavelength of the input signal. The time delay between the centre of the array and the mth microphone is written as

$$\tau_m = \frac{r}{c}\cos(\theta - \psi_m) \tag{4.1}$$

where

$$\psi_m = \frac{2\pi(m-1)}{M} \tag{4.2}$$

The microphones are arranged on a circle with radius r. The distance between two successive sensors is then

$$\delta = 2r\sin(\frac{\pi}{M}) \approx \frac{2\pi r}{M} \tag{4.3}$$

The steering vector of length M can now be written as

$$\begin{aligned}\mathbf{d}(\omega,\theta) &= [e^{j\omega\tau_1} \quad e^{j\omega\tau_2} \quad \dots \quad e^{j\omega\tau_M}]^T \\ &= [e^{j\omega\frac{r}{c}\cos(\theta-\psi_1)} \quad e^{j\omega\frac{r}{c}\cos(\theta-\psi_2)} \quad \dots \quad e^{j\omega\frac{r}{c}\cos(\theta-\psi_M)}]^T\end{aligned} \tag{4.4}$$

It is supposed that the desired signal comes from the angle $\theta = \theta_s$. In analogy to Sec. 2.2 the mth microphone signal is written as

$$X_m(\omega) = S(\omega)e^{j\omega\frac{r}{c}\cos(\theta_s-\psi_m)} + V_m(\omega), \qquad m = 1,2,\dots,M \tag{4.5}$$

The beamformer output of a UCA for an angular frequency ω at target direction θ_s is

$$\begin{aligned}Y(\omega) &= \sum_{m=1}^{M} H_m^*(\omega,\theta_s)X_m(\omega) \\ &= \mathbf{h}^H(\omega,\theta_s)\mathbf{d}(\omega,\theta_s)S(\omega) + \mathbf{h}^H(\omega,\theta_s)\mathbf{v}(\omega)\end{aligned} \tag{4.6}$$

where superscripts * and ^{H} denote complex conjugation and conjugate-transpose operator. The beamforming filter of length M is rewritten as

$$\mathbf{h}(\omega) = [H_1(\omega) \quad H_2(\omega) \ \dots \ H_M(\omega)]^T \tag{4.7}$$

where superscript ^{T} is the transpose operator.

Beampattern

The beampattern describes the sensitivity of the beamformer to a plane wave impinging on the array from direction θ.

$$\begin{aligned}\mathcal{B}(\omega,\theta_s,\theta) &= \mathbf{h}^H(\omega,\theta_s)\mathbf{d}(\omega,\theta) \\ &= \sum_{m=1}^{M} \mathbf{H}_m^*(\omega,\theta_s)e^{j\omega\frac{r}{c}\cos(\theta-\psi_m)}\end{aligned} \tag{4.8}$$

Directivity Factor and Directivity Index

The directivity factor of an Nth order CDMA is

$$\mathcal{G}_N(\theta_s) = \frac{\mathcal{B}_N^2(0)}{\frac{1}{\pi}\int_{\theta_s}^{\theta_s+\pi} \mathcal{B}_N^2(\theta-\theta_s)d\theta} \tag{4.9}$$

The Directivity index is defined as

$$\mathcal{D}_N(\theta_s) = 10\log_{10}\mathcal{G}_N(\theta_s) \tag{4.10}$$

4.2 First-Order Circular Differential Array

The first-order CDMA is designed with $M = 3$ microphones. The geometry of the CDMA is then an equilateral triangle with the positions of the microphones lying at:

$$\psi_1 = 0, \quad \psi_2 = \frac{2\pi}{3} \quad \psi_3 = \frac{4\pi}{3} \tag{4.11}$$

It is supposed that the desired signal is at the angle $\theta_s = 0°$. As there are $M = 3$ microphones a set of M linear equations has to be solved resulting in M constraints which have to be fulfilled. First, distortionless response at the angle $\theta = 0°$, second, a null is steered at the angle of $\theta = \theta_{1,1}$ with $0 < \theta_{1,1} \leq \pi$. The third constraint implies that the beampattern is symmetric according to $H_2(\omega) = H_3(\omega)$. In matrix notation the constraints can be written as

$$\begin{bmatrix} \mathbf{d}^H(\omega, 0) \\ \mathbf{d}^H(\omega, \theta_{1,1}) \\ \mathbf{c}_{3,1}^T \end{bmatrix} \mathbf{h}(\omega) = \begin{bmatrix} 1 \\ \beta_{1,1} \\ \beta_{1,1} \end{bmatrix} \tag{4.12}$$

where $\mathbf{c}_{3,1} = [0 \quad 1 \quad -1]^T$. Rewriting Eq. (4.12) with $\theta_{1,1}$ and $\beta_{1,1} = 0$ to

$$\underbrace{\begin{bmatrix} e^{-j\omega\frac{r}{c}} & e^{-j\omega\frac{r}{c}\cos\psi_2} & e^{-j\omega\frac{r}{c}\cos\psi_3} \\ e^{-j\omega\frac{r}{c}\cos(\theta_{1,1})} & e^{-j\omega\frac{r}{c}\cos(\theta_{1,1}-\psi_2)} & e^{-j\omega\frac{r}{c}\cos(\theta_{1,1}-\psi_3)} \\ 0 & 1 & -1 \end{bmatrix}}_{\mathbf{A}_3(\omega,\theta)} \mathbf{h}(\omega) = \underbrace{\begin{bmatrix} 1 \\ 0 \\ 0 \end{bmatrix}}_{\mathbf{b}_3} \tag{4.13}$$

the beamforming filter is then calculated by

$$\mathbf{h}(\omega) = \mathbf{A}_3^{-1}(\omega, \theta)\mathbf{b}_3 \tag{4.14}$$

The calculation of the first-order CDMA beampattern leads to

$$|\mathcal{B}(\omega, \theta)|^2 = |\mathbf{d}^H(\omega, \theta)\mathbf{A}_3^{-1}(\omega, \theta)\mathbf{b}_3|^2 \tag{4.15}$$

In Fig. 4.2 the beampattern of a first-order CDMA with different $\theta_{1,1}$ is depicted.

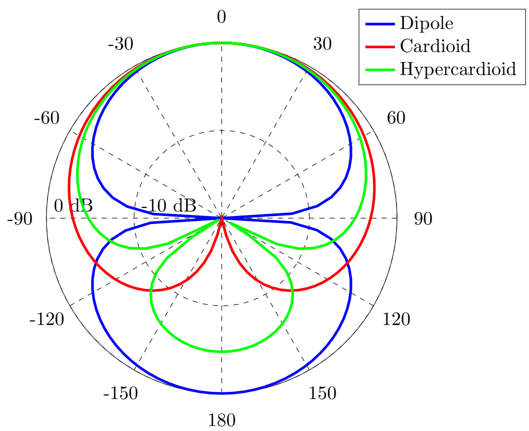

Figure 4.2: Different beampatterns of a first-order CDMA for $f = 1000Hz$.

The values for $\theta_{1,1}$ for the previous beampatterns are:

- Dipole: $\theta_{1,1} = 90°$
- Cardioid: $\theta_{1,1} = 180°$
- Hypercardioid: $\theta_{1,1} = 120°$

4.2.1 Frequency Response of First-Order CDMA

Fig. 4.3 shows the frequency response for a first-order CDMA with radius $r = 0.01m$. The directional response for direction $\theta = 0°$ is frequency-independent for the whole frequency range. For signals impinging from other directions, the directional response is frequency-independent only at low frequency range. For higher frequencies, the shape gets more and more deformed.

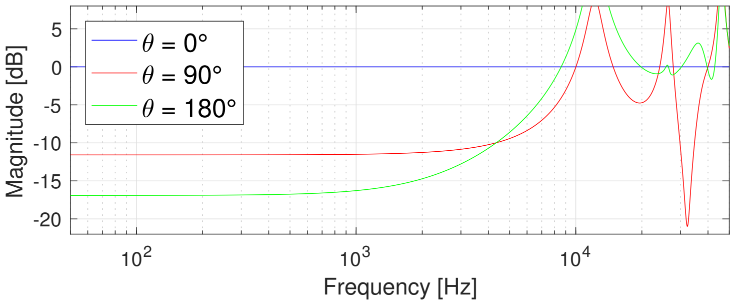

Figure 4.3: Frequency response of a first-order CDMA with radius $r = 0.01m$

4.3 Second-Order Beamformer for Hearing Aid Geometry

The microphones of a hearing aid are arranged in line on the left and the right side of the artificial head (cf. 4.4b). The basic idea is to adapt the geometry of a circular array to the geometry of the hearing aids for both sides. To do so, the time delay τ_m between the mth microphone and the centre of the array has to be modified. Fig. 4.4 shows the schematic of the geometry used for further calculations. Fig. 4.4a depicts the xy-plane whereas Fig. 4.4b shows the yz-plane, respectively.

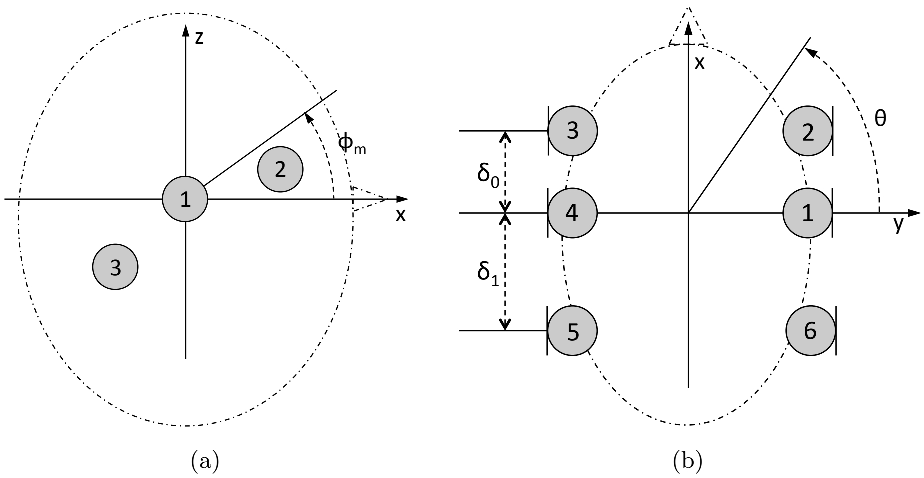

Figure 4.4: Schematic of the six microphones arranged at the artificial head: (a) view of the right side, (b) view from the top.

The time delays are calculated as:

$$\tau_{m,n} = \frac{1}{c}(-x\cos\phi\cos\theta_n - y\cos\phi\sin\theta_n - z\sin\phi) \tag{4.16}$$

where x,y and z are the coordinates of the microphones in Cartesian coordinates and θ_n and ϕ representing the direction of the desired signal impinging on the array.

The array consists of $M = 6$ microphones. In analogy to the previous chapters, it would be possible to solve M linear equations resulting in M constraints to be fulfilled. This would result in a third-order CDMA. As the symmetry constraint is neglected, which is described later on, only three constraints remain. First, a one is steered at $\theta = 0°$, second, two nulls are steered at the angles $\theta_{2,1}$ and $\theta_{2,2}$. The result is an under-determined linear system which has to be solved.

$$\begin{bmatrix} \mathbf{d}^H(\omega, 0) \\ \mathbf{d}^H(\omega, \theta_{2,1}) \\ \mathbf{d}^H(\omega, \theta_{2,2}) \end{bmatrix} \mathbf{h}(\omega) = \begin{bmatrix} 1 \\ \beta_{2,1} \\ \beta_{2,2} \end{bmatrix} \tag{4.17}$$

$$\underbrace{\begin{bmatrix} e^{-j\omega\tau_{1,1}} & e^{-j\omega\tau_{1,2}} & e^{-j\omega\tau_{1,3}} & e^{-j\omega\tau_{1,4}} & e^{-j\omega\tau_{1,5}} & e^{-j\omega\tau_{1,6}} \\ e^{-j\omega\tau_{2,1}} & e^{-j\omega\tau_{2,2}} & e^{-j\omega\tau_{2,3}} & e^{-j\omega\tau_{2,4}} & e^{-j\omega\tau_{2,5}} & e^{-j\omega\tau_{2,6}} \\ e^{-j\omega\tau_{3,1}} & e^{-j\omega\tau_{3,2}} & e^{-j\omega\tau_{3,3}} & e^{-j\omega\tau_{3,4}} & e^{-j\omega\tau_{3,5}} & e^{-j\omega\tau_{3,6}} \end{bmatrix}}_{\mathbf{A}_3(\omega,\theta)} \mathbf{h}(\omega) = \underbrace{\begin{bmatrix} 1 \\ 0 \\ 0 \end{bmatrix}}_{\mathbf{b}_3} \tag{4.18}$$

In analogy to Sec. 4.2 the second-order beampattern is calculated as

$$|\mathcal{B}(\omega, \theta)|^2 = |\mathbf{d}^H(\omega, \theta)\mathbf{A}_3^{-1}(\omega, \theta)\mathbf{b}_3|^2 \tag{4.19}$$

According to Fig. 4.4a, the microphones of the hearing aid do not lie exactly in the xz-plane. In the previous chapters, the elevation angle ϕ has been neglected. For the second-order beamformer with six microphones it is taken into account as the differences are relevant for further calculations. Fig. 4.5a depicts the beampatterns calculated with an elevation angle $\phi = 0°$ but without the symmetry constraint. Especially for Cardioid 2 it is obvious that the attenuation is not that much as in Fig. 4.6 and the cardioid is not symmetric at all. The symmetry constraint as well as the elevation angle $\phi \approx 19°$ are taken into account at Fig. 4.5b. The beampatterns are symmetric for all cardioids but the steering direction $\theta = 0°$ is completely attenuated which is not useful for implementation.

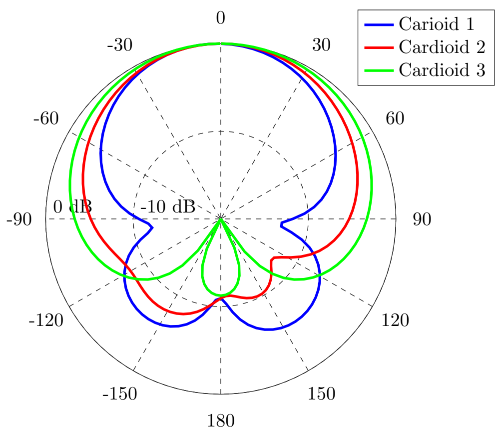

(a)

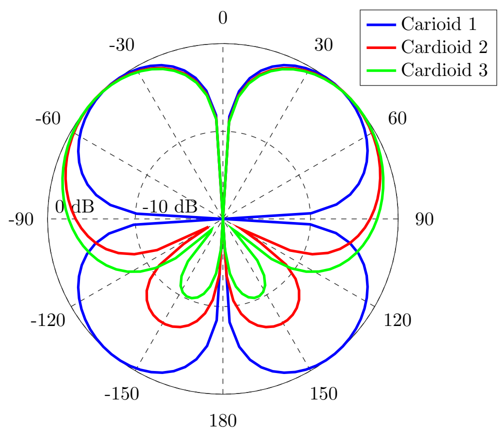

(b)

Figure 4.5: Beampatterns of second-order beamformer for hearing aid geometry for $f = 1000Hz$: (a) elevation angle $\phi = 0°$ and no symmetry constraint (b) elevation angle $\phi \approx 19°$ and with symmetry constraint.

Based on these assumptions the symmetry constraint is neglected and an elevation angle of $\phi = 0°$ is chosen for further calculations. The results are depicted in Fig. 4.6.

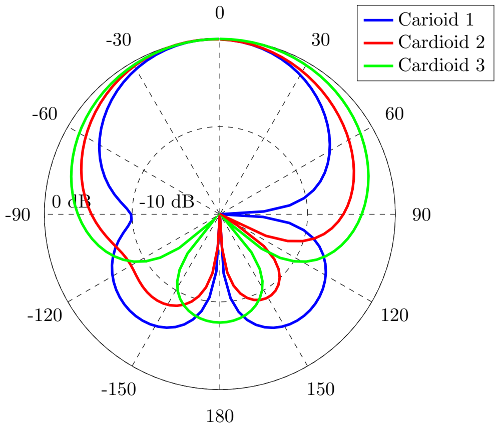

(a)

Figure 4.6: Beampatterns of second-order beamformer for hearing aid geometry for $f = 1000Hz$: (a) elevation angle $\phi = 0$, (b) elevation angle $\phi \approx 19°$.

The values for $\theta_{2,1}$ and $\theta_{2,2}$ of the previous beampatterns are:

- Cardioid 1: $\theta_{2,1} = 90°$ and $\theta_{2,2} = 180°$
- Cardioid 2: $\theta_{2,1} = 120°$ and $\theta_{2,2} = 180°$
- Cardioid 3: $\theta_{2,1} = 135°$ and $\theta_{2,2} = 225°$

In real situations it is not practical that the source direction has to impinge on the array with an elevation angle of $\phi > 0°$. Therefore, to use a beamformer with six microphones arranged at an artificial head, the geometry should be adapted for practical use to achieve the best performance. The illustration of the beamformer in a 3D-plot, shown in Fig. 4.7, is more significant to evaluate the steering direction.

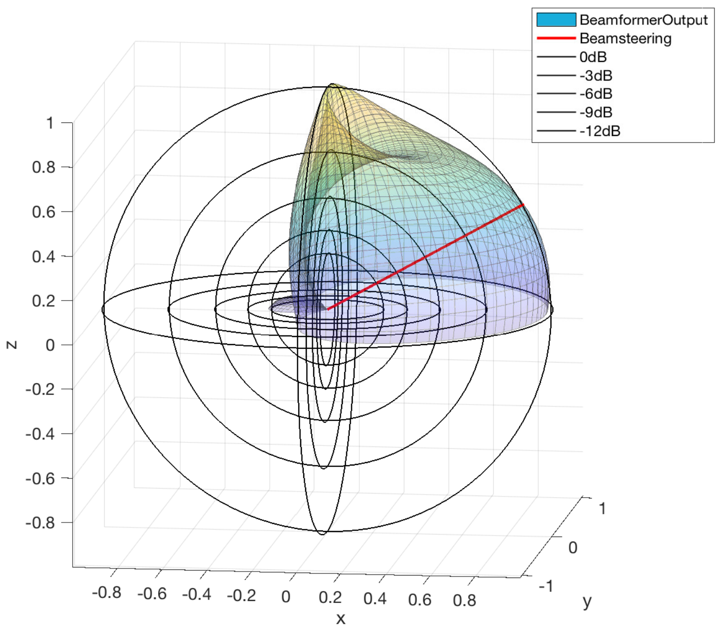

Figure 4.7: Beampattern of second-order beamformer for hearing aid geometry for $f = 1000Hz$.

4.3.1 Frequency Response of Second-Order Beamformer

In Fig. 4.8 the directional response of the second-order beamformer for hearing aid geometry is depicted. For a steering direction $\theta = 0°$ the directional response is frequency-independent for the whole frequency range as expected. For all other steering directions the directional response is attenuated but still has a frequency-independent characteristic in the low frequency range. For higher frequencies $f > 1000Hz$ the frequency response is highly non-linear.

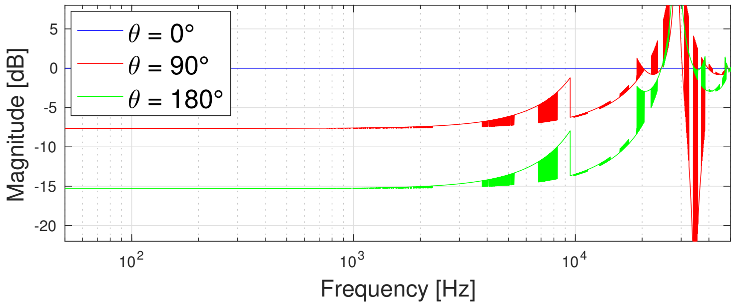

Figure 4.8: Frequency response of a second-order beamformer for hearing aid geometry.

5 Postfilter

In this chapter different calculations for postfilters are discussed. A detailed overview of the structures is given and the advantages and disadvantages are revealed.

5.1 Introduction

In the previous chapters different beamforming techniques have been discussed generating a single-channel output signal for each ear (bilateral hearing aid). As the aim is a binaural system preserving binaural cues, the output signal has to be binauralized in a postfiltering step. In binaural spectral postfiltering techniques, the frequency bins of the short-time Fourier transform (STFT) are weighted with a real-valued gain in order to retain the target source and to suppress interfering sources. Although binaural spectral postfiltering techniques increase speech intelligibility and spatial source localization, they also introduce speech distortion and artefacts [13]. In the following chapters different binaural postfiltering techniques working with differential microphone array outputs are introduced.

5.2 Postfilter Estimation using Cardioids $PF_{\textsf{Card}}$

One binaural postfiltering technique is the comparison between the frequency bins of the short-time Fourier transform between two processing channels. A gain close to one is applied when the STFT bin should be retained, i.e. at the target source, and a gain close to zero is applied when the STFT bin should be suppressed, i.e. at interfering sources and noise [13]. The output of the comparison between two processing channels is a so called speech mask, containing real-valued gains for each STFT bin. The estimated speech mask is taken as a postfilter.
In this approach, the forward- and backward-facing cardioid have been used as processing channels. In ideal conditions the forward cardioid should mainly contain the target signal, while the backward cardioid should only contain noise and interfering sources. The spectral gain of the speech mask for each frequency bin is now computed by comparison between each STFT bin of the two cardioids. If the power spectrum of the STFT bin of the forward cardioid is greater than the equivalent bin of the backward cardioid, a value of one is set to the corresponding speech mask bin, otherwise, a value of 0.3 is set to the appropriate bin in the speech mask.
The schematic structure of the whole process using an adaptive beamforming algorithm and a

postfilter is depicted in Fig. 5.1. The output signals $y(l, k_f)$ and $c(l, k_f)$ denote the STFTs of the respective time-domain signals with l representing the frame index and k_f representing the frequency bin index.

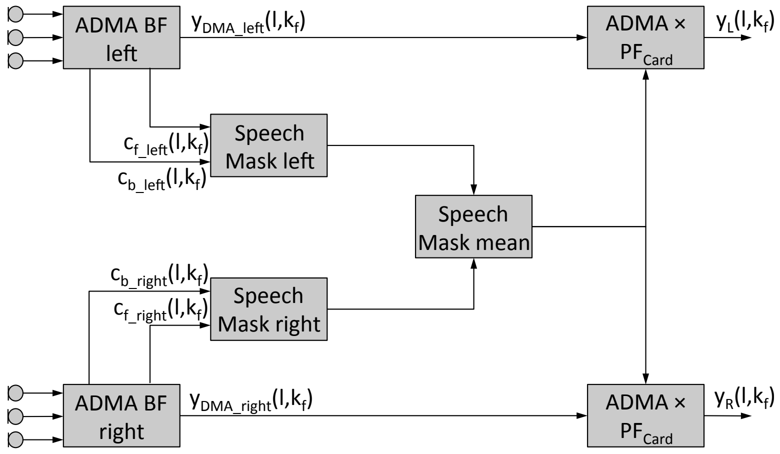

Figure 5.1: Schematic of postfilter structure using forward- and backward-facing cardioid of DMA.

In Fig. 5.2a and 5.2b the short-time Fourier transform of the forward and backward cardioid are shown. After comparison, the speech mask containing static values for each frequency bin is shown in Fig. 5.2c.

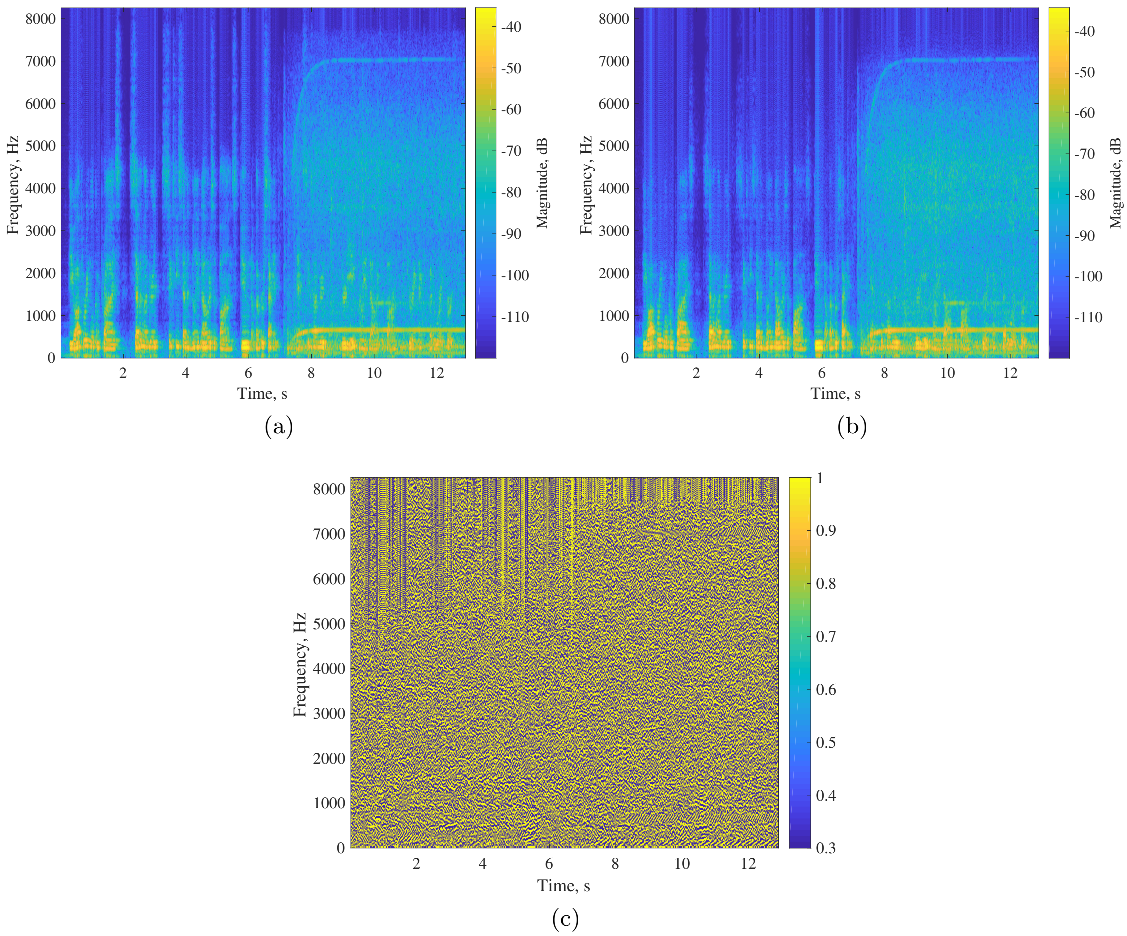

Figure 5.2: Spectrogram of left side: (a) forward cardioid, (b) backward cardioid, (c) static speech mask

As shown in Fig. 5.1 the average of the left and the right speech mask is taken and multiplied with the output of the left and the right beamformed signal. Chapter 6 gives an evaluation of the output signal according to speech intelligibility, noise reduction and binaural cue preservation.

5.3 Postfilter Estimation using Signal-to-Noise Ratio PF_{SNR}

In contrast to the static estimation of the speech mask, another approach is obtained in [14]. The estimation of the gain is computed by an a priori and an a posteriori SNR. The overall gain for each frequency bin is estimated by

$$\mathcal{G} = \frac{A_k}{R_k} = \frac{\xi_k}{1+\xi_k} e^{\frac{1}{2}\int_{v_k}^{\infty} \frac{e^{-t}}{t} dt} \tag{5.1}$$

where A_k is the estimation of the amplitude, R_k is the noisy observation, v_k is defined by $v_k = \frac{\xi_k}{1+\xi_k}\gamma_k$. ξ_k and γ_k representing the a priori and a posteriori signal-to-noise ratio, respectively. The schematic structure which has been used for evaluation is shown in Fig. 5.3.

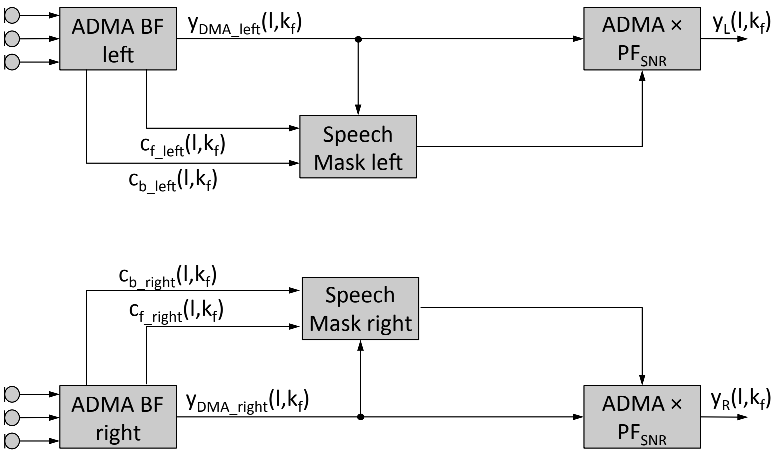

Figure 5.3: Schematic of postfilter structure using SNR estimation.

In this approach the a priori SNR is computed by the power spectrum of the forward- and backward-facing cardioid. The a posteriori SNR is the quotient of the power spectrum of the beamformer output and the backward cardioid. Nevertheless, this method causes a lot of artefacts and musical noise in the overall beamformer output.

5.4 Postfilter Estimation using Fixed Beamformer $PF_{\mathbf{6Mic}}$

To get a better preservation of the binaural cues, an additional second-order beamformer proposed in Sec. 4.3 is used for speech mask estimation. The real-valued gains have been estimated in the same way as described in Sec. 5.2. The frequency bins of the STFT have been compared between the output of the fixed beamformer using six microphones and the backward-facing cardioid of the adaptive beamformer for the left and right signal respectively. If the power spectrum of the STFT bin of the fixed beamformer is greater than the equivalent bin of the adaptive beamformer, a one is set to the corresponding speech mask bin, otherwise, a value of 0.5 is set to the appropriate bin in the speech mask. Again, the resulting speech mask only contains static values. The schematic structure which is used for this speech mask estimation is shown in Fig. 5.4.

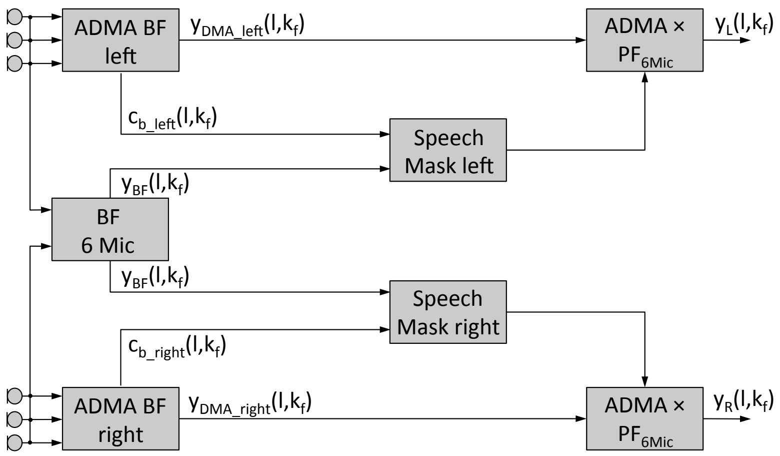

Figure 5.4: Schematic of postfilter structure using an additional beamformer.

5.5 Postfilter Estimation using Coherence $PF_{\mathbf{Coh}}$

One last approach of a speech mask estimation used in this study is the gain estimation by using the coherence function. The coherence measures the correlation between two signals at the frequency ω. The result is a real-valued number between $0 \leq \mathcal{C}_{xy}(\omega) \leq 1$. The coherence between two signals is calculated by

$$\mathcal{C}_{xy}(\omega) = \frac{|P_{xy}(\omega)|^2}{P_{xx}(\omega)P_{yy}(\omega)} \tag{5.2}$$

where $\mathcal{P}_{xy}(f)$ is the cross-power spectral density between x and y and $P_{xx}(f)$ and $P_{yy}(f)$ are the power spectral density respectively of x and y. In this approach the speech mask of the adaptive beamformer output of right and left channel are compared to form an overall speech mask output. The estimated speech mask is again multiplied with each output signal of the adaptive beamformer as shown in Fig. 5.5.

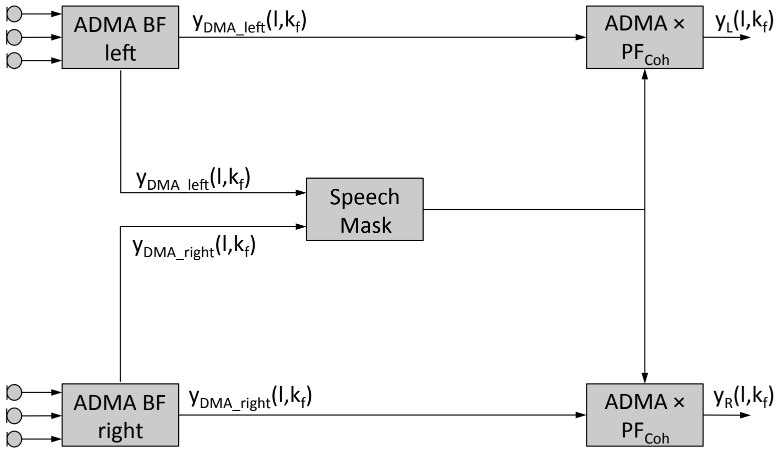

Figure 5.5: Schematic of postfilter structure using a coherence function.

5.6 Postfilter Processing on One Microphone

In the previous sections, a detailed description of the speech mask estimation is given. It is supposed that the resulting postfilter is always used for the output signal of the adaptive beamformer. Another approach is the use of the postfilter only on a single microphone signal for each side. The estimation of the speech mask stays the same as mentioned in the previous sections. The schematic structure is depicted in Fig. 5.6.

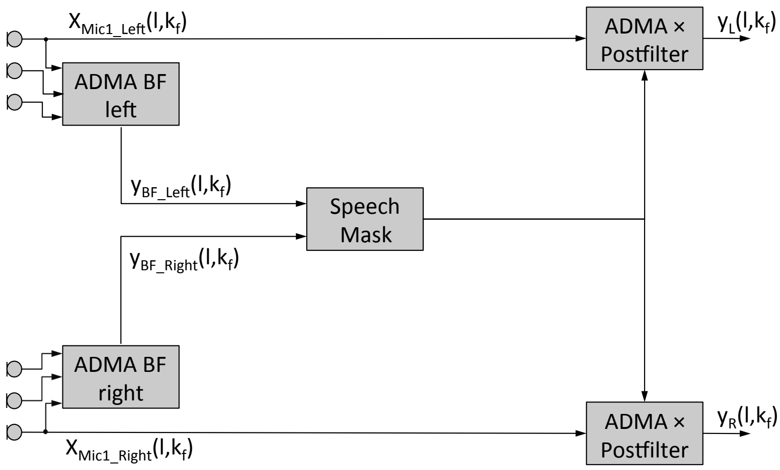

Figure 5.6: Schematic of postfilter structure used on a single microphone signal for each side.

6 Evaluation

The provided algorithms for a use in a hearing aid are evaluated in this chapter. The main focus lies on the estimation of speech intelligibility, noise reduction and binaural cue preservation parameters. A description of the audio data and the head-related impulse response used for evaluation of the provided algorithms is given.

6.1 Audio Data

The ChiMe2 [15] and ChiMe3 [16] database is used for input signals. The database provides a huge amount of high-quality clean speech signals with male and female speakers and background noise signals. The background noise is chosen in terms of realistic localisation conditions. Three different background noises, namely a vacuum cleaner interferer, music interferer and street-sound interferer, were chosen. The vacuum cleaner interferer is a recording of a vacuum cleaner in-use. The music interferer contains synthetic music sounds and the street-sound interferer comprises a car driving sound. To simulate an input signal consisting of speech and noise both signals have been added. The following table shows the input signals and the corresponding direction.

	Signal	Direction
	Vacuum Cleaner Interferer	
Target	Male Speaker	0°
Background	Vacuum Cleaner	90°
	Music Interferer	
Target	Male Speaker	0°
Background	Music	90°
	Street-Sound Interferer	
Target	Female Speaker	0°
Background	Car	0°

Table 6.1: Definition of input signals and source directions.

6.2 HRIR Database

To provide a real sound field for simulation, the anechoic input signals have been convolved with a head-related impulse response (HRIR). The HRIR database is provided by [3]. The recordings have been made with a human head and torso simulator *Brüel & Kjær Type 4128C* with artificial ears. The impulse responses were measured with a three-channel behind-the-ear hearing aid and an in-ear microphone at both ears. For this study only the HRIRs of the hearing aid dummy have been used. The geometry of the microphones for the right side of the artificial head are shown in Fig. 6.1. This arrangement has been used for the evaluation.

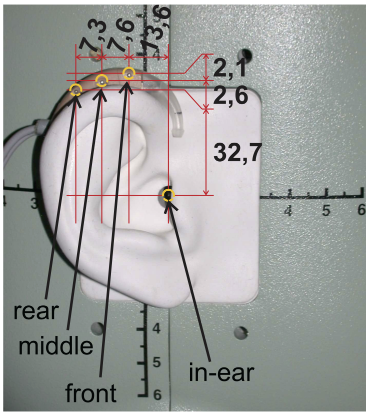

Figure 6.1: Brüel & Kjær artificial head with hearing aid dummy (right side) [3].

The database provides impulse responses in natural environments as well as a measurement in an anechoic chamber. For this study only anechoic HRIRs with a sampling frequency of $f_s = 48000kHz$ are used, reverberant situations have been left out.

6.3 Evaluation of Signal-to-Noise Ratio

The input SNR is calculated by the clean speech and noise signal which are independently available. Table 6.2 shows the original values.

	Original SNR [dB]		
	Vacuum Cleaner Interferer	Music Interferer	Street-Sound Interferer
left	4.7	4.3	-7.2
right	-4.0	-0.4	-4.9

Table 6.2: Calculation of input SNR.

More difficult is the calculation of the output SNR as the output signal of the beamformer is a mixture of the speech and noise component. To calculate the output SNR it is necessary to separate the output signal into a speech signal component and a noise signal component. The speech estimation is calculated by means of the coherence function used in Sec. 5.5. The coherence between the clean speech and output signal is calculated and the result is multiplied with the output signal. The same steps have been done for the noise estimation respectively. The best results are achieved with a temporal smoothing coefficient of 0.01.
A significant improvement of SNR is achieved by cutting of the low frequency range ($f < 150Hz$) as there is the major amplification of the white noise gain. An increase of up to 3dB is achieved. In the following sections the detailed results are discussed.

Comparison of ADMA Beamformer

The evaluation between different adaptive differential microphone arrays is proposed in Tab. 6.3. Precisely, a comparison between the second-order ADMA (SO) and the hybrid structure of frequency and level dependence (f_{Hyb} and L_{Hyb}) is made. In addition, one postfilter PF_{Card} is used after the adaptive beamformer. Tab. 6.3 shows the result of the Δ SNR calculated between the input and the output SNR.

	Vacuum Cleaner Interferer					
	SO	f_{Hyb}	L_{Hyb}	SO+PF_{Card}	f_{Hyb}+PF_{Card}	L_{Hyb}+PF_{Card}
Δ SNR left [dB]	-2.4	1.9	1.8	0.8	**3.3**	**3.3**
Δ SNR right [dB]	9.0	9.7	9.7	10.6	**11.5**	**11.5**
	Music Interferer					
	SO	f_{Hyb}	L_{Hyb}	SO+PF_{Card}	f_{Hyb}+PF_{Card}	L_{Hyb}+PF_{Card}
Δ SNR left [dB]	2.1	**4.5**	4.2	2.6	4.5	4.2
Δ SNR right [dB]	7.3	**9.3**	8.9	7.6	9.2	9.0
	Street-Sound Interferer					
	SO	f_{Hyb}	L_{Hyb}	SO+PF_{Card}	f_{Hyb}+PF_{Card}	L_{Hyb}+PF_{Card}
Δ SNR left [dB]	3.4	**4.0**	**4.0**	2.9	3.6	3.6
Δ SNR right [dB]	3.3	**4.2**	**4.2**	2.5	3.7	3.7

Table 6.3: Evaluation of different adaptive beamformer.

The vacuum cleaner and music interferer impinge from the right side on the array. Therefore, the SNR improvement is clearly bigger for the right side than for the left one. In comparison, the increase in SNR for the street-sound interferer is the same for both sides because both signals, the speaker and interferer, come from the same direction.
The best performance reveals the hybrid structure, similarly for frequency and level dependence. An additional improvement by the postfilter provides only the result of the vacuum cleaner interferer.

Comparison of Postfilter

The evaluation between different postfilters is shown in Table 6.4. As adaptive beamformer the hybrid structure of level dependence is used. A comparison between the four postfilters proposed in chapter 5, namely PF_{Card}, PF_{SNR}, PF_{6Mic} and PF_{Coh}, is made. Again the results show the calculated Δ SNR.
It is interesting, that for each interferer a different postfilter performs best, although there are only small differences between them. It is remarkable that the PF_{Coh} performs best for the street-sound interferer as this filter introduces a lot of artefacts, which is shown in Sec. 6.4.

	Vacuum Cleaner Interferer			
	PF_{Card}	PF_{SNR}	PF_{6Mic}	PF_{Coh}
Δ SNR left [dB]	**3.3**	3.3	1.8	1.0
Δ SNR right [dB]	**11.5**	11.2	10.3	8.5
	Music Interferer			
	PF_{Card}	PF_{SNR}	PF_{6Mic}	PF_{Coh}
Δ SNR left [dB]	4.2	**4.2**	3.9	3.6
Δ SNR right [dB]	9.0	**9.2**	8.8	8.3
	Street-Sound Interferer			
	PF_{Card}	PF_{SNR}	PF_{6Mic}	PF_{Coh}
Δ SNR left [dB]	3.6	3.2	3.9	**6.0**
Δ SNR right [dB]	3.7	3.8	4.2	**6.4**

Table 6.4: Evaluation of different postfilters.

Output to One Microphone

Table 6.5 shows the comparison between the postfilters applied to a single microphone signal for each side. As the PF_{Coh} introduces a lot of artefacts and noise interference, it is left out for this comparison.
The SNR improvement for music and street-sound interferer is nearly the same as in Tab. 6.4. This means there is just a minor difference between the performance of an adaptive beamformer plus a postfilter compared to a single postfilter. The result of the vacuum cleaner interferer is unexpected as the SNR decreases for the left side.

	Vacuum Cleaner Interferer		
	PF_{Card}	PF_{SNR}	PF_{6Mic}
Δ SNR left [dB]	**-2.1**	-1.6	-5.2
Δ SNR right [dB]	**2.9**	0.8	0.4
	Music Interferer		
	PF_{Card}	PF_{SNR}	PF_{6Mic}
Δ SNR left [dB]	3.8	**3.8**	3.3
Δ SNR right [dB]	8.4	**8.5**	7.9
	Street-Sound Interferer		
	PF_{Card}	PF_{SNR}	PF_{6Mic}
Δ SNR left [dB]	3.4	3.0	**3.7**
Δ SNR right [dB]	3.4	3.5	**3.8**

Table 6.5: Evaluation of postfilters applied to a single microphone signal for each side.

In conclusion, the results reveal a good performance for both hybrid structures. Using an additional postfilter, PF_{Card} and PF_{SNR} show the best results in terms of SNR improvement. It is shown that the SNR improvement increases if the target and interfering signal do not impinge from the same direction.

6.4 Evaluation with PEASS-Software

The PEASS-Software is a toolkit provided by [17] and [18]. It measures different objective scores for the evaluation of audio source separation. It is assumed that the original source signals are known. The maximum score which can be achieved is 100. There are four perceptually motivated quality scores which are used in the following evaluation:

1. Overall Perceptual Score (OPS): rates the global quality compared to the reference signal
2. Target-related Perceptual Score (TPS): rates the quality in terms of preservation of the target source
3. Interference-related Perceptual Score (IPS): rates the quality in terms of suppression of other sources
4. Artefact-related Perceptual Score (APS): rates the quality in terms of absence of additional artificial noise

The original quality scores of the input signal of one microphone are:

	Original Quality Scores		
	Vacuum Cleaner Interferer	Music Interferer	Street-Sound Interferer
OPS	8	8	8
TPS	63	75	82
IPS	8	5	1
APS	85	87	87

Table 6.6: Calculation of input SNR.

Comparison of ADMA Beamformer

The evaluation between different adaptive beamformer with and without an additional postfilter is shown in Tab. 6.7. The results compare different Δ quality scores calculated between the processed and the original signal.
The aim of beamforming techniques is to retain the target signal while suppressing interfering sources. The results of music and vacuum cleaner interferer confirm this aim. The target-related perceptual score stays nearly the same which is expected because the target signal has very good quality. The interfering-perceptual score increases meaning that interfering sources are clearly suppressed. The artefact-related perceptual score decreases, especially for the second-order adaptive beamformer, which is expected as the postfiltering technique introduces speech distortion and artefacts (cf. Sec 5.1). The overall-perceptual score increases slightly which is the desired result.
Remarkable are the results of the street-sound interferer. Although the SNR increases for this signal (cf. Tab. 6.3) the quality scores do not confirm this result. This might be due to the same direction of target and interfering source.
The best performance reveals the hybrid structure of frequency dependence and level dependence for all interferer.

	Vacuum Cleaner Interferer					
	SO	f_{Hyb}	L_{Hyb}	SO+PF_{Card}	f_{Hyb}+PF_{Card}	L_{Hyb}+PF_{Card}
Δ OPS	27	24	24	27	**39**	32
Δ TPS	-2	-6	-8	-4	**3**	-3
Δ IPS	64	70	36	66	**75**	49
Δ APS	-49	-5	-24	-48	**-6**	-26
	Music Interferer					
	SO	f_{Hyb}	L_{Hyb}	SO+PF_{Card}	f_{Hyb}+PF_{Card}	L_{Hyb}+PF_{Card}
Δ OPS	33	11	30	34	**19**	39
Δ TPS	-18	-16	-13	-19	**4**	-12
Δ IPS	64	62	42	68	**68**	58
Δ APS	-41	-8	-26	-42	**-12**	-26
	Street-Sound Interferer					
	SO	f_{Hyb}	L_{Hyb}	SO+PF_{Card}	f_{Hyb}+PF_{Card}	L_{Hyb}+PF_{Card}
Δ OPS	11	0	0	11	0	0
Δ TPS	-53	-1	0	-46	0	-1
Δ IPS	25	0	0	24	0	0
Δ APS	-57	0	0	-58	0	0

Table 6.7: Evaluation of different adaptive beamformer with PEASS Software.

Comparison of Postfilter

The comparison between different postfilters is shown in Tab. 6.8. The evaluated postfilters are PF_{Card}, PF_{SNR}, PF_{6Mic} and PF_{Coh}. Again the hybrid structure of level dependence is used as adaptive beamformer.

	Vacuum Cleaner Interferer			
	PF_{Card}	PF_{SNR}	PF_{6Mic}	PF_{Coh}
Δ OPS	32	**41**	31	32
Δ TPS	-3	**-2**	-4	-19
Δ IPS	49	**57**	45	56
Δ APS	-26	**-27**	-25	-43
	Music Interferer			
	PF_{Card}	PF_{SNR}	PF_{6Mic}	PF_{Coh}
ΔOPS	39	39	31	32
Δ TPS	-12	-12	-12	-29
Δ IPS	58	59	44	55
Δ APS	-26	-25	-27	-43
	Street-Sound Interferer			
	PF_{Card}	PF_{SNR}	PF_{6Mic}	PF_{Coh}
Δ OPS	0	0	0	12
Δ TPS	-1	-12	-10	-55
Δ IPS	0	0	0	10
Δ APS	0	-1	-1	-34

Table 6.8: Evaluation of different postfilters with PEASS Software.

All postfilters introduce a lot of artefacts especially the postfilter estimation using the coherence function. For all other quality scores there is no significant difference between the postfilters but the PF_{Card} and PF_{SNR} show the best results for all interferer. The interference suppression is very good for music and vacuum cleaner interferer which confirms the results of Tab. 6.7.

Output to One Microphone

Table 6.9 shows the results between the postfilters applied to a single microphone signal for each side.

	Vacuum Cleaner Interferer		
	PF_{Card}	PF_{SNR}	PF_{6Mic}
Δ OPS	0	9	0
Δ TPS	-4	-14	4
Δ IPS	13	24	5
Δ APS	2	-12	2
	Music Interferer		
	PF_{Card}	PF_{SNR}	PF_{6Mic}
Δ OPS	0	0	0
Δ TPS	-13	-11	-7
Δ IPS	12	10	4
Δ APS	0	0	0
	Street-Sound Interferer		
	PF_{Card}	PF_{SNR}	PF_{6Mic}
Δ OPS	0	0	0
Δ TPS	0	-1	-1
Δ IPS	0	0	0
Δ APS	0	0	0

Table 6.9: Evaluation of postfilters applied to a single microphone signal for each side.

For the street-sound interferer there is no difference between all evaluated methods as all quality scores remain nearly the same.
In contrast to the evaluation of SNR, the results between Tab. 6.9 and Tab. 6.8 differ a lot for the music and vacuum cleaner interferer. The performance of an adaptive beamformer and an additional postfilter is obviously better than the performance of a postfilter alone. Especially the interference-related perceptual score reveals that the interference suppression is better for the process of an adaptive beamformer and a postfilter. Nevertheless, it it remarkable that there are nearly no artefacts introduced by a postfilter alone.

Summarizing, the results of the PEASS Software confirm the conclusion of the SNR evaluation. The PF_{Card} and PF_{SNR} perform best in terms of interfering source suppression and target preservation. Although, the postfilter applied to a single microphone signal slightly improve the SNR, the results of the PEASS Software for these postfilters do not confirm an interfering source suppression.

6.5 Perceptual Evaluation

The evaluation of the binaural cue preservation is done by a listening test. The stimuli setup is shown in the following Tab. 6.10.

	Signal	Direction				
	Vacuum Cleaner Interferer					
Target	Male Speaker	0°				
Background	Vacuum Cleaner	90°	45°	0°	−45°	−90°
	Music Interferer					
Target	Male Speaker	0°				
Background	Music	90°	45°	0°	−45°	−90°
	Street-Sound Interferer					
Target	Female Speaker	0°				
Background	Car	90°	45°	0°	−45°	−90°

Table 6.10: Direction of different presented stimuli.

The speaker direction did not change and remained in the direction $\theta = 0°$. The background noise is varied between $-90° < \theta < 90°$ within steps of 45°. All interfering signals, vacuum cleaner interferer, music interferer and street-sound interferer, have been tested. They were randomly presented to the listener by headphones. Seven normal-hearing listeners aged between 28 and 59 participated. The listeners have been asked to evaluate from which direction they perceive the speech and interfering signal. Both signals have been evaluated separately within five discrete angles described in Tab. 6.10.

Results of Different Angles

To evaluate the results the error angle between the original and the measured angle is calculated. The errors which can occur are listed in Tab. 6.11. For Fig. 6.2 the absolute values of errors are taken for evaluation.

		Measured Angle				
		-90	-45	0	45	90
Original Angle	-90	0	45	90	135	180
	-45	-45	0	45	90	135
	0	-90	-45	0	45	90
	45	-135	-90	-45	0	45
	90	-180	-135	-90	-45	0

Table 6.11: Possible Angles of error observation.

Fig. 6.2a shows the result of the original signal for each tested angle. It is obvious that the most errors occur for the presented angles of −45° and 45°. This means the background noise is rather observed from the left and the right side. As the microphones of the hearing aid are placed behind the ear, it is possible that the source localisation is thereby limited. Besides, the background noise coming from the front has no distinctive observed direction.

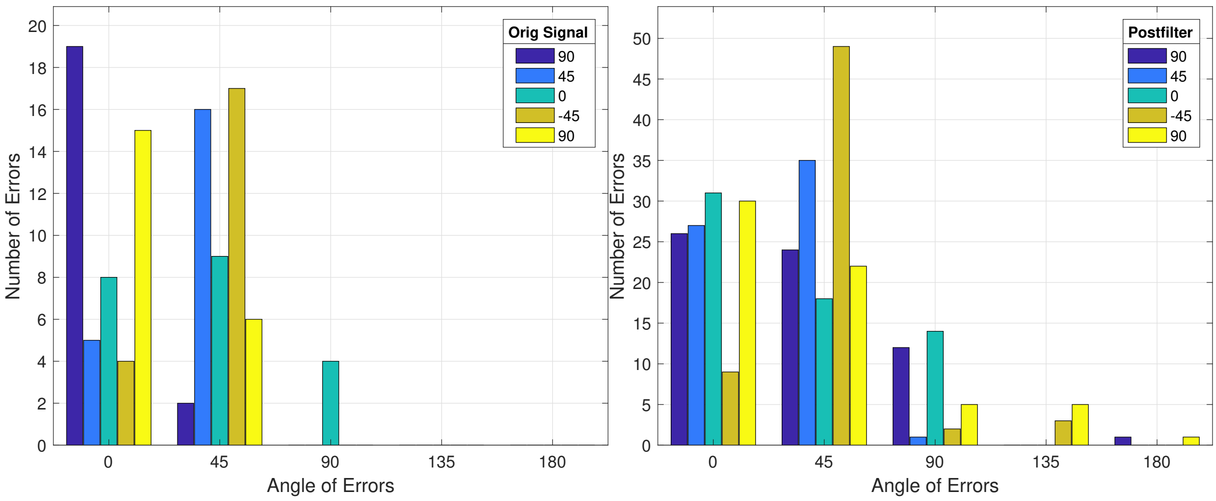

(a) (b)

Figure 6.2: Absolute values of errors for background signals over all input signals for each tested angle: (a) errors of original signal, (b) errors of all postfilters.

To preserve the binaural cues the results of the tested postfilters should be similar to the result of the original signal shown in Fig. 6.2b. The errors of the angles $-45°$ and $45°$ stay nearly the same as for the original signal whereas the error of the $0°$ direction decreases. Although the variation of the results increases, the most errors occur between $0°$ and $45°$. This means a source localization after the beamforming algorithm is still possible and is preserved in comparison to the original signal. A detailed listing for each postfilter and tested angle is shown in appendix B.

Results of Different Postfilters

The result of the original signal over all tested angles in Fig. 6.3a shows a normal distribution which is expected according to Tab. 6.11. The results of all postfilters should be similar if the binaural cues are preserved.

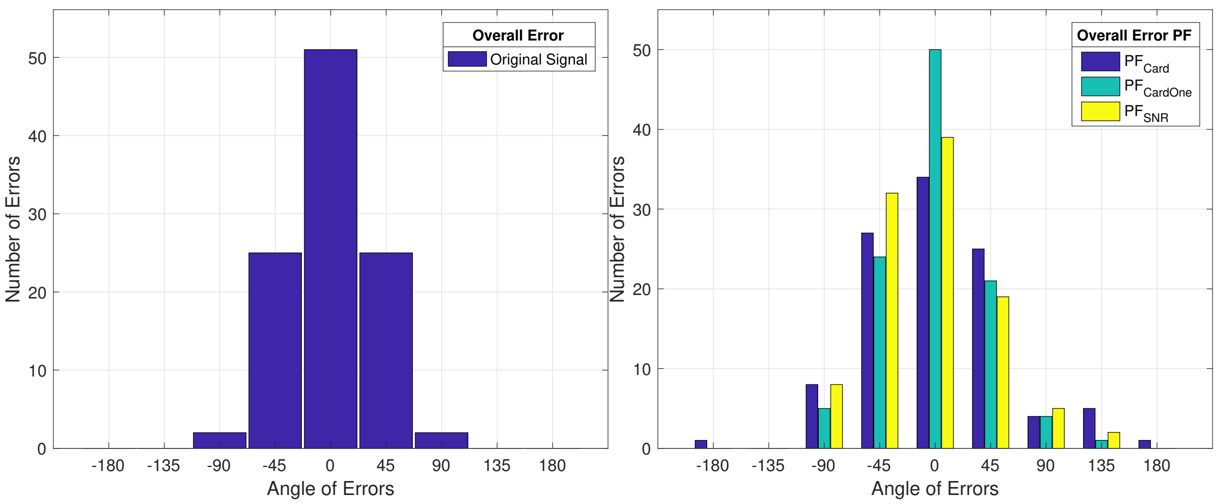

(a) (b)

Figure 6.3: Errors of background signals over all input signals and tested angles : (a) result of original input signal (b) result of different postfilters.

Although the variation increases, a normal distribution is observed for all postfilters and shown in Fig. 6.3b. The best result is given by the postfilter $PF_{CardOne}$. Corresponding to [13] there is always a trade-off between suppression of interfering sources and preservation of localisation cues. This trade-off is clearly visible for $PF_{CardOne}$ as the results of SNR reveal less increase, the results of the binaural cue preservation are so much the better. A detailed listing of all results for each tested interfering signal is given in appendix B.

Conclusion

The results in chapter 6 reveal that the hybrid structures perform best in terms of noise reduction. Using an additional beamformer, the postfilters PF_{Card} and PF_{SNR} achieved the best results for interfering source suppression and target preservation. Regarding binaural cue preservation the postfilter $PF_{CardOne}$ introduces the least errors. However, the SNR improvement and suppression of interfering sources is clearly worse than for the other tested postfilter. Therefore, the postfilters PF_{Card} and PF_{SNR} give a good compromise between noise reduction, interfering suppression and binaural cue preservation.

7 Conclusion and Outlook

In this master's thesis different beamforming algorithms based on differential microphone arrays for the use in a hearing aid have been investigated. The main focus lied on the enhancement of speech intelligibility by simultaneously preserving binaural cues. Differential microphone arrays have the potential to steer nulls in specific directions while preserving a target signal over a wide frequency range coming from another direction. They use a compact sensor arrangement which is profitable for the use in a hearing aid.
A specific geometry of a hearing aid dummy was used. The calculations had to be adapted to the arrangement of the microphone setup. Precisely, the microphone distances have not be equally spaced leading to different time delays between two successive sensors. Nevertheless, there has been no specific difference in the directional beampattern for equally or unequally spaced microphone for differential microphone arrays.
To improve the speech intelligibility by simultaneously preserving binaural cues, different binaural spectral postfiltering techniques have been proposed. One idea has been the adaptation of a circular differential microphone array to the array geometry of a hearing aid using six microphones. Although this specific postfilter achieved good results in consideration of noise reduction a restriction in binaural cue preservation was observed by an informal evaluation by the author.
Different input signals simulating real situations have been chosen to evaluate the proposed algorithms. The best results of signal-to-noise ratio improvement have been achieved by the hybrid structures. The results did not provide an obvious increase in SNR with an additional postfilter. The results of the evaluation in terms of interfering source suppression have always been better with a postfilter than without. The postfilter applied to a single microphone signal achieved the best results in matters of binaural cue preservation. The results reveal that there is always a trade-off between noise reduction performance and binaural cue preservation. Nevertheless, the hybrid structures with a postfilter estimation using cardioids reveal a good compromise between speech enhancement and binaural cue preservation.
All proposed algorithms have been tested under ideal conditions as the speech and noise signals have been convolved with an anechoic impulse response. For realistic scenarios reverberation has to take into account to test the proposed algorithms to its robustness. Based on these results further investigation can be made for postfiltering techniques. One idea is the estimation of a postfilter by using deep neuronal networks (e.g. [19]). At the moment these methods are still very complex in its computational effort and not appropriate for real-time implementations. This is one of the advantages of the proposed algorithms as the computational effort is low.

Bibliography

[1] M. L. Hawley, R. Y. Litovsky, and J. F. Culling, “The benefit of binaural hearing in a cocktail party: Effect of location and type of interferer”, *The Journal of the Acoustical Society of America*, vol. 115, no. 2, pp. 833–843, 2004.

[2] J. Peissig and B. Kollmeier, “Directivity of binaural noise reduction in spatial multiple noise-source arrangements for normal and impaired listeners”, *The Journal of the Acoustical Society of America*, vol. 101, no. 3, pp. 1660–1670, 1997.

[3] H. Kayser, S. D. Ewert, J. Anemüller, T. Rohdenburg, V. Hohmann, and B. Kollmeier, “Database of multichannel in-ear and behind-the-ear head-related and binaural room impulse responses”, *EURASIP Journal on Advances in Signal Processing*, vol. 2009, p. 6, 2009.

[4] T. J. Klasen, T. Van den Bogaert, M. Moonen, and J. Wouters, “Binaural noise reduction algorithms for hearing aids that preserve interaural time delay cues”, *IEEE Transactions on Signal Processing*, vol. 55, no. 4, pp. 1579–1585, 2007.

[5] MATLAB, `http://www.mathworks.com/`.

[6] J. Benesty and C. Jingdong, “Study and design of differential microphone arrays”, *Springer Science & Business Media*, vol. 6, 2012.

[7] G. W. Elko and A.-T. N. Pong, “A simple adaptive first-order differential microphone”, *IEEE ASSP Acoustic Workshop on Applications of Signal Processing to Audio and Acoustics*, pp. 169–172, 1995.

[8] E. Messner, “Differential microphone arrays”, Master’s Thesis, Graz University of Technology, Austria, 2013.

[9] G. Moschytz and M. Hofbauer, “Adaptive filter”, *Springer Verlag Berlin*, 2000.

[10] G. W. Elko and J. Meyer, “Second-order differential adaptive microphone array”, *IEEE International Conference on Acoustics, Speech and Signal Processing, ICASSP*, pp. 73–76, 2009.

[11] V. Hamacher, E. Fischer, U. Kornagel, and H. Puder, “Applications of adaptive signal processing methods in high-end hearing aids”, *Topics Acoustic Echo and Noise Control*, pp. 599–636, 2006.

[12] J. Benesty, J. Chen, and I. Cohen, “Design of circular differential microphone arrays”, *Springer Science & Business Media*, vol. 6, 2015.

[13] S. Doclo, W. Kellermann, S. Makino, and S. E. Nordholm, “Multichannel signal enhancement algorithms for assisted listening devices: Exploiting spatial diversity using multiple microphones”, *IEEE Signal Processing Magazine*, vol. 32, no. 2, pp. 18–30, 2015.

[14] Y. Ephraim and D. Malah, “Speech enhancement using a minimum mean-square error log-spectral amplitude estimator”, *IEEE Transactions on Acoustics, Speech, and Signal Processing*, vol. 33, no. 2, pp. 443–445, 1985.

[15] E. Vincent, J. Barker, S. Watanabe, J. Le Roux, F. Nesta, and M. Matassoni, “The second ‘chime’ speech separation and recognition challenge: Datasets, tasks and baselines”, *IEEE International Conference on Acoustics, Speech and Signal Processing (ICASSP)*, pp. 126–130, 2013.

[16] J. Barker, E. Vincent, N. Ma, H. Christensen, and P. Green, “The pascal chime speech separation and recognition challenge”, *Computer speech & language*, vol. 27, no. 3, pp. 621–633, 2013.

[17] V. Emiya, E. Vincent, N. Harlander, and V. Hohmann, “Subjective and objective quality assessment of audio source separation”, *IEEE Transactions on Audio, Speech, and Language Processing*, vol. 19, no. 7, pp. 2046–2057, 2011.

[18] E. Vincent, “Improved perceptual metrics for the evaluation of audio source separation”, *International Conference on Latent Variable Analysis and Signal Separation*, pp. 430–437, 2012.

[19] L. Pfeifenberger, T. Schrank, M. Zohrer, M. Hagmüller, and F. Pernkopf, “Multi-channel speech processing architectures for noise robust speech recognition: 3rd chime challenge results”, *IEEE Workshop on Automatic Speech Recognition and Understanding (ASRU)*, pp. 452–459, 2015.

A

Results of Listening Test

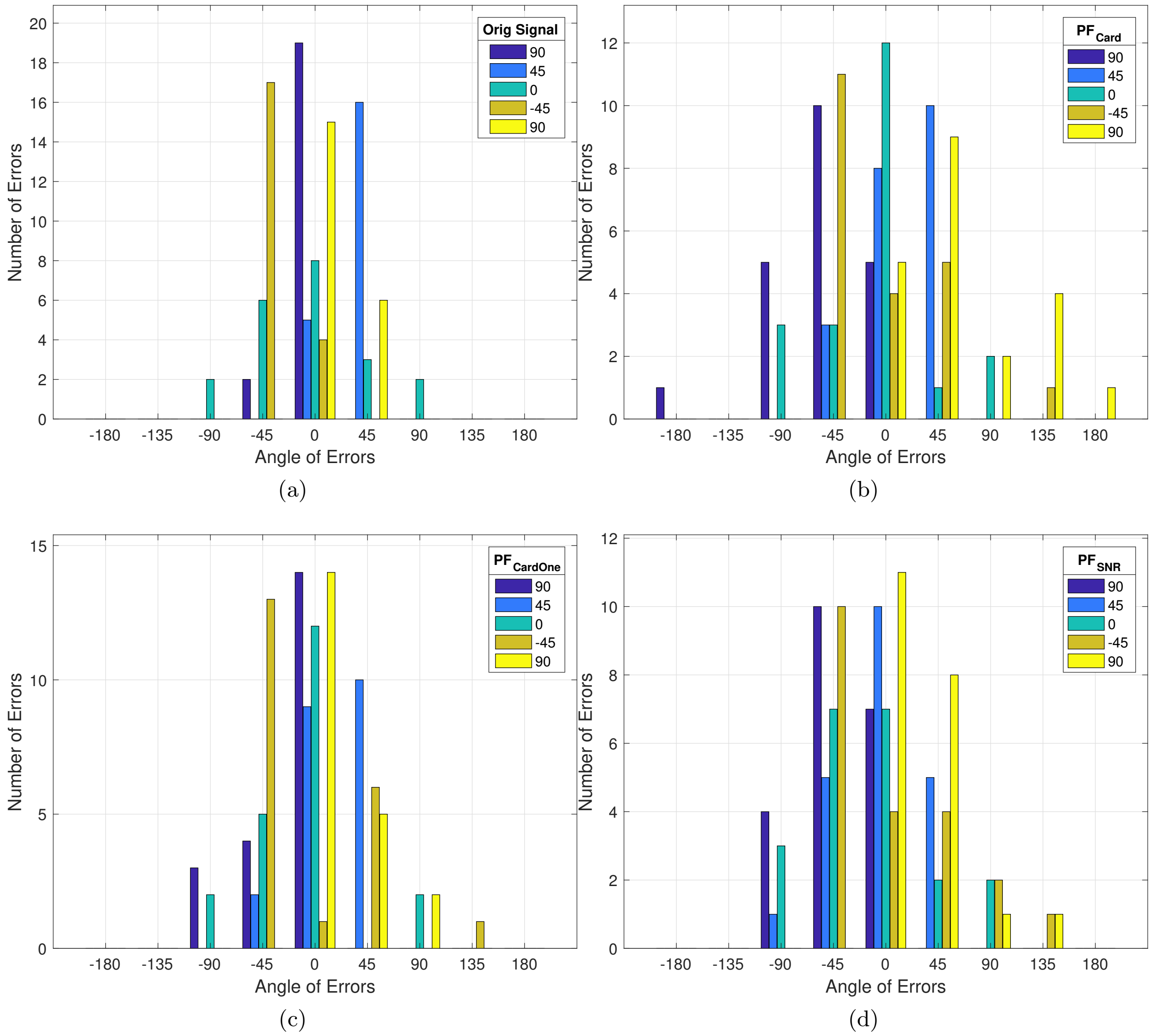

Figure A.1: Errors of background signals over all input signals for each tested angle: (a) result of original signal, (b) result of PF_{Card}, (c) result of $PF_{CardOne}$, (d) result of PF_{SNR}.

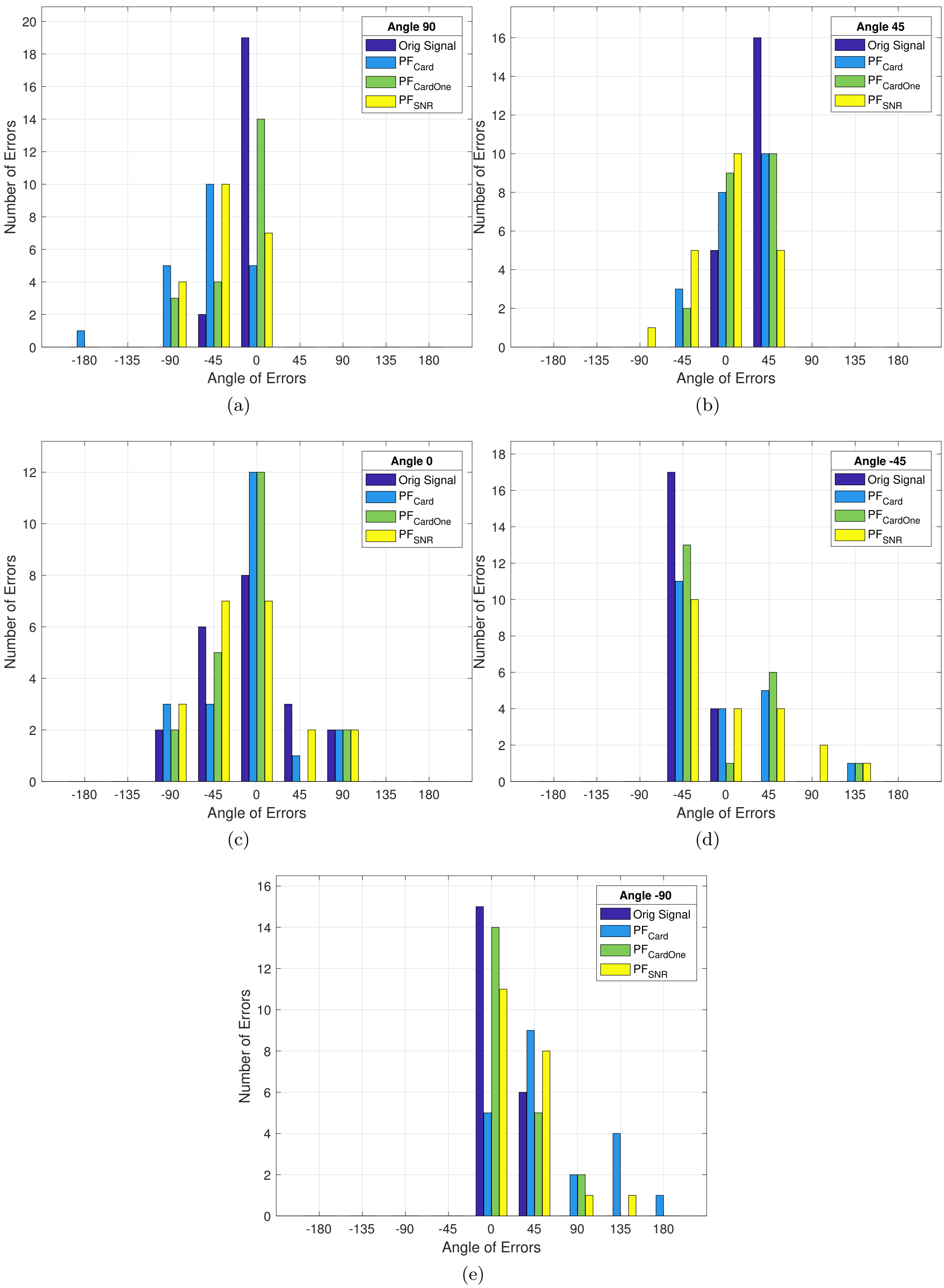

Figure A.2: Errors of background signals over all input signals for each tested postfilter compared to the original input signals: (a) result of angle 90°, (b) result of angle 45°, (c) result of angle 0°, (d) result of angle −45°, (e) result of angle −90°.

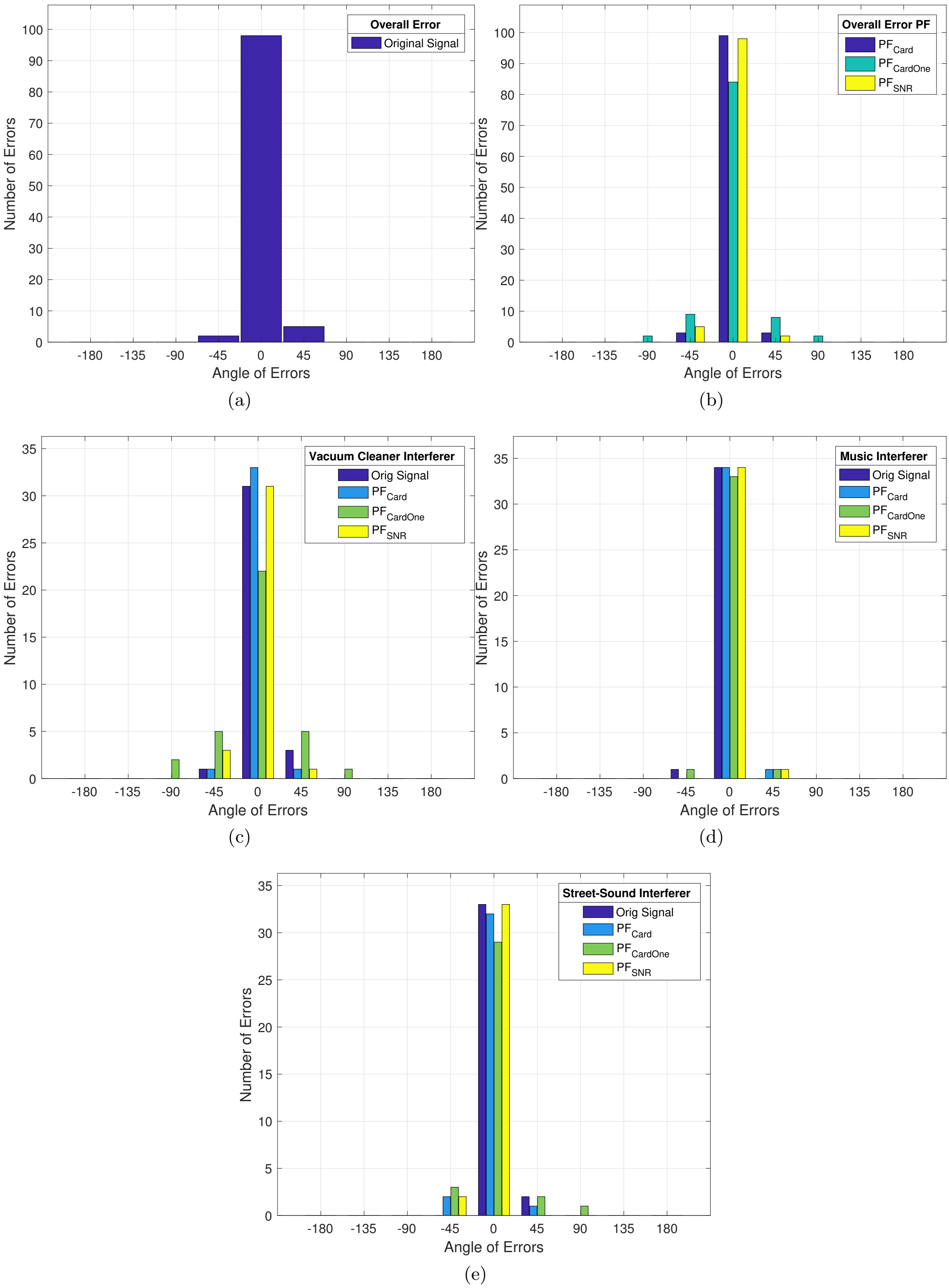

Figure A.3: Errors of speech signals over all angles: (a) overall result of all input signals, (b) overall result of each postfilter for all input signals, (c) result of vacuum cleaner interferer for each postfilter, (d) result of music interferer for each postfilter, (e) result of street-sound interferer for each postfilter.

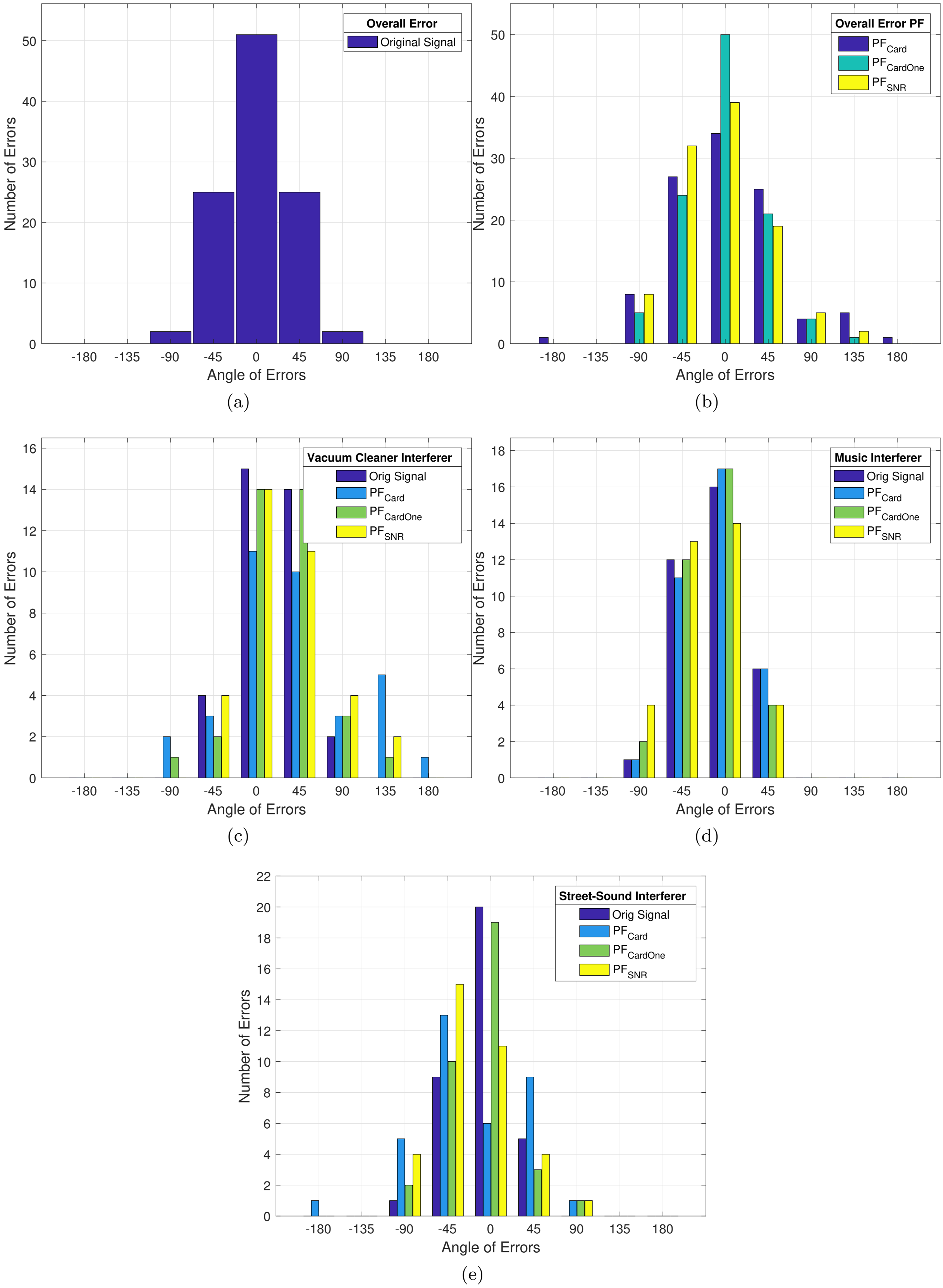

Figure A.4: Errors of background signals over all angles: (a) overall result of all input signals, (b) overall result of each postfilter for all input signals, (c) result of vacuum cleaner interferer for each postfilter, (d) result of music interferer for each postfilter, (e) result of street-sound interferer for each postfilter.

B

Abbreviations

ADMA	Adaptive Differential Microphone Array
APS	Artefact-related Perceptual Score
CDMA	Circular Differential Microphone Array
BF	Beamformer
DMA	Differential Microphone Array
HRIR	Head-related Impulse Response
IPS	Interference Perceptual Score
NLMS	Normalized Least Mean Square algorithm
OPS	Overall Perceptual Score
PF_{6Mic}	Postfilter Estimation using Six Microphones
PF_{Card}	Postfilter Estimation using Cardioid
PF_{Coh}	Postfilter Estimation using Coherence
PF_{SNR}	Postfilter Estimation using SNR
SNR	Signal-to-Noise Ratio
SRM	Spatial Release from Masking
STFT	short-time Fourier transform
TPS	Target Perceptual Score
UCA	Uniform Circular Array
ULA	Uniform Linear Array
WNG	White Noise Gain

C Symbols

δ	distance between two successive sensors
λ	wave length
ω	angular frequency
ω_c	angular cut-off frequency
ϕ	elevation angle
μ_0	constant step-size
μ	adaptive step-size
τ_0	time delay between two successive sensors at the angle $\theta = 0°$
τ_m	time delay between two successive sensors
θ	azimuth angle
θ_s	source incidence angle
c	propagation speed of sound
f	temporal frequency
f_N	Nyquist-Frequency
f_s	sampling frequency
k	time index
k_f	frequency bin index
l	frame index
M	number of microphones
m	microphone index
N	order of DMA
r	radius
$H_L(\omega)$	compensation filter
$H_m(\omega, \theta_s)$	mth filter element of source direction θ_s

$s(k), S(\omega)$	source signal in time and frequency domain
$v_m(k), V_m(\omega)$	additive noise at the mth microphone signal in time and frequency domain
$x_m(k), X_m(\omega)$	mth microphone signal in time and frequency domain
$y(k), Y(\omega)$	beamforming output in time and frequency domain
$\mathcal{B}$	beampattern
$\mathcal{G}_N(\theta)$	directivity factor of direction θ
$\mathcal{D}_N(\theta)$	directivity index of direction θ
$\mathbf{A}(\omega, \theta)$	steering matrix
$\mathbf{b}$	steering coefficient vector
$\mathbf{c}$	symmetry constraint vector
$\mathbf{d}(\omega, \theta)$	steering vector
$\mathbf{h}(\omega)$	filter vector
$\mathbf{v}(\omega)$	noise signal vector
$\mathbf{x}(\omega)$	signal vector
$\alpha_{N,n}$	design coefficient for the null steering direction of Nth order DMA
$\beta_{N,n}$	design coefficient for the value of the null steering direction of Nth order DMA
$\theta_{N,n}$	design coefficient for the angle of the null steering direction of Nth order DMA
α_1	steering coefficient of second-order ADMA
α_2	steering coefficient of second-order ADMA
β	steering coefficient of first-order ADMA
$c_b(t), C_b(\omega, \theta)$	first-order backward-facing cardioid in time and frequency domain
$c_bb(t), C_bb(\omega, \theta)$	second-order backward-facing cardioid in time and frequency domain
$c_f(t), C_f(\omega, \theta)$	first-order forward-facing cardioid in time and frequency domain
$c_ff(t), C_ff(\omega, \theta)$	second-order forward-facing cardioid in time and frequency domain
$c_tt(t), C_t(\omega, \theta)$	second-order toroid in time and frequency domain
$e(t)$	error signal
Δ	regularization parameter
$P_{c_bc_b}(0)$	power of the backward-facing cardioid
$P_{c_fc_f}(0)$	power of the forward-facing cardioid
$P_{c_fc_b}(0)$	cross-power between the forward-facing cardioid
$P_{xx}(\omega)$	power spectral density of x
$P_{yy}(\omega)$	power spectral density of y
$P_{xy}(\omega)$	cross-power spectral density between x and y
A_k	amplitude estimation
R_k	noise observation
ξ_k	a priori SNR
γ_k	a posteriori SNR